



**JOÃO CARLOS
MARTINS TEIXEIRA**

**SENSIBILIDADE DO WRF À FRONTEIRA INFERIOR E
PARAMETRIZAÇÕES URBANAS**

**WRF SENSITIVITY TO LOWER BOUNDARY AND URBAN
CANOPY PARAMETRIZATIONS**



**JOÃO CARLOS
MARTINS TEIXEIRA**

**SENSIBILIDADE DO WRF À FRONTEIRA INFERIOR E
PARAMETRIZAÇÕES URBANAS**

**WRF SENSITIVITY TO LOWER BOUNDARY AND URBAN
CANOPY PARAMETRIZATIONS**

Dissertação apresentada à Universidade de Aveiro para cumprimento dos requisitos necessários à obtenção do grau de Mestre em Meteorologia e Oceanografia Física, realizada sob a orientação científica de Alfredo Rocha, Professor do Departamento Física da Universidade de Aveiro e Ana Cristina Carvalho, Investigadora Auxiliar do CENSE-FCT-UNL, Centro de Investigação em Ambiente e Sustentabilidade, Faculdade de Ciências e Tecnologia Universidade Nova de Lisboa.

o júri / the jury

presidente / president

Professor Doutor José Manuel Henriques Castanheira

Professor auxiliar da Universidade de Aveiro

vogais / examiners committee

Professor Doutor João Alexandre Medina Corte-Real

Professor catedrático aposentado da Universidade de Évora

Professor Doutor Alfredo Moreira Caseiro Rocha

Professor associado com agregação da Universidade de Aveiro

Doutora Ana Cristina Caldeira da Silva Gouveia Carvalho

Investigadora auxiliar da Faculdade de Ciências e Tecnologia da Universidade Nova de Lisboa

**agradecimentos /
acknowledgements**

Aproveito esta oportunidade para agradecer aos meus orientadores, Professor Doutor Alfredo Rocha e Doutora Ana Cristina Carvalho, pelas oportunidades e por todo o apoio que me deram ao longo do desenvolvimento deste trabalho, bem como ao Tiago Luna e Susana Vaz pela disponibilidade e ajuda que prontamente me prestaram. Agradeço também ao Laboratório Regional de Engenharia Civil e à Direção Regional de Informação Geográfica da Região Autónoma da Madeira pelo fornecimento dos dados que auxiliaram na realização deste trabalho. Aproveito também para agradecer aos meus pais e à Maria João Carvalho, por sempre me apoiarem em tudo o que foi necessário. Finalmente, aproveito para agradecer a todos os meus colegas que, mesmo tendo que suportar o meu desinteresse pelas tarefas mundanas do dia-a-dia, sempre me apoiaram.

Palavras Chave

modelos de mesoescala, fronteira inferior, precipitação extrema, parametrizações urbanas

Resumo

Ao longo dos anos avanços, na tecnologia de satélite viabilizaram a aquisição de informações sobre a superfície da Terra, tais como elevação e uso do solo, com grande detalhe e resolução. Esta informação pode ser incluída em modelos numérico da atmosfera, atualizando e dando-lhes mais detalhes sobre as condições de fronteira inferior. Assim sendo, este trabalho visa estudar a sensibilidade do Weather Research and Forecasting model a três conjuntos de dados de topografia, e dois de uso do solo diferentes. Um caso de estudo em que a precipitação orográfica foi dominante sobre a Ilha da Madeira foi considerado mostrando que, em geral não existe um aumento significativo da performance do modelo ao usar topografia ou uso do solo de alta resolução. Contudo, existe uma melhor performance do modelo em simular a precipitação a barlavento e o fluxo a sotavento da ilha. Dada a natureza deste estudo, considerou-se também um teste à sensibilidade de três parametrizações de microfísica, sendo que os resultados encontrados não mostram alterações significativas aos resultados encontrados. Além disso, a introdução de um novo conjunto de dados de uso do solo tornou possível realizar simulações usando modelos urbanos acoplados. Assim, de forma a estudar a sensibilidade a estes modelos considerou-se um caso de estudo sobre a região de Lisboa. Ao utilizar um modelo urbano verificou-se que sobre a região urbana existe um arrefecimento à superfície quando comparando com as simulações de controlo. Além disso verificou-se uma grande diferença no escoamento e na energia turbulenta produzida sobre esta zona. Estas diferenças podem por sua vez interagir com ondas gravíticas, alterando a sua fase e amplitude. Além disso, ao comparar os resultados com dados observados verificou-se que, em geral, não existe melhoria na performance do modelo para este caso de estudo. No entanto o uso do modelo urbano BEP melhora significativamente os resultados relativos à altura da camada de mistura.

Key Words

mesoscale models, lower boundary, extreme precipitation, urban parametrizations

Abstract

Through the years, the advances in satellite technology made feasible the acquisition of information about the Earth surface, such as elevation and land use, with great detail and resolution. This information can be included in numerical atmospheric models, updating and giving them more details about the lower boundary. Given so, this work aims to study the sensitivity of the Weather Research and Forecast model to three different topography datasets as well as two different land use datasets. A test case study in which topography driven precipitation was dominant over Madeira Island was considered. Overall, results show that there is no enhancement of model skill when using higher resolution topography or land use. However, there is a higher model skill simulating precipitation on Madeira leeward and wind flow windward. Additionally, given the nature of this event, a sensitivity test was also performed considering three different microphysics parametrizations. This test showed that the choice of the microphysics parametrizations does not significantly change the results found for this event. Furthermore, the introduction of a new land use dataset turned possible to perform simulations using Urban Canopy Models. Therefore, the sensitivity of the model to these urban parametrizations was also performed. In this work, a case study for the Lisbon region was chosen and showed that the simulations that used a urban canopy model presented a cooling in the urban region. Moreover, larger changes were observed for wind flow and turbulence kinetic energy over the area. In addition, it was shown that these could change the phase and amplitude of gravity waves that were generated in the region. When comparing to observed data it was seen that there is no enhancement of model skill when using these models. However, the planetary boundary layer is better represent by BEP urban model.

Contents

1	Introduction	1
I	Model Sensitivity to Lower Boundary Conditions and Microphysics. Weather precipitation event	3
2	State of The Art	4
3	Method and Data	6
4	Results and Discussion	10
4.1	Synoptic Setting	10
4.2	Sensitivity to Topography	10
4.2.1	Topography datasets	10
4.2.2	Wind modelled data	11
4.2.3	Precipitation modelled results	13
4.3	Sensitivity to Land Use	15
4.4	Modelled results vs Observed data	17
4.5	Microphysics Sensitivity	22
4.6	Synthesis	23
II	Model Sensitivity to Lower Boundary Conditions and Urban Parametriza- tions. High pressure weather pattern	25
5	State of The Art	26
6	Method and Data	28
7	Results and Discussion	33
7.1	Atmospheric Situation	33
7.2	Sensitivity to the UCMs	35
7.3	Modelled results vs Observed data	40
7.3.1	Surface Observations	41
7.3.2	Radiosonde Observations	41
7.4	Synthesis	43
8	Concluding Remarks	45

List of Figures

3.1	Study area map showing the Madeira archipelago location in the Atlantic Ocean, Maps from googlemaps.com.	6
3.2	Three nested model domains used in WRF.	7
3.3	Location of the weather stations in Madeira Island (blue dotted - Portuguese Meteorological Institute; White dotted - Madeira Regional Civil Engineer Laboratory) and the location of the cross section used in this work (red line).	8
4.1	Synoptic situation for February 20 th at 12:00 UTC (ERA Interim, daily fields)	10
4.2	Vertical cross section for Brunt-Väisälä frequency (s^{-1}) for February 20 th at 12:00 UTC control simulation.	11
4.3	Topography field for CTL simulation (m) and topography cross section for the three data sets, CTL (red), SRTM (blue) and ASTER (black) simulations, and difference fields (m) between both high resolution topography data sets and the control topography for domain d03 at a resolution of one kilometre.	12
4.4	Wind direction (arrows) and intensity (shaded) ($m \cdot s^{-1}$) for the horizontal wind components at a ten meter height of February 20 th at 12 UTC for the CTL simulation at 06 and 12 UTC.	13
4.5	Difference field for intensity ($m \cdot s^{-1}$) at a ten meter high (shaded) between SRTM and ASTER with CTL simulations and wind direction for SRTM and ASTER (red arrows) and CTL simulations (black arrows) for February 20 th at 12 UTC.	13
4.6	Difference field for mean wind intensity ($m \cdot s^{-1}$) at a ten meter height between SRTM and ASTER with CTL simulations for February 20 th	14
4.7	Accumulated precipitation ($mm \cdot day^{-1}$) for February 20 th in domain d03 for control simulation.	14
4.8	Difference fields for accumulated precipitation ($mm \cdot day^{-1}$) between both - SRTM and ASTER simulations - and the CTL simulation for February 20 th	15
4.9	USGS land use categories field used on the CTL simulation.	16
4.10	USGS land use categories field based on the CORINE land use dataset.	16
4.11	Difference fields between CORINE and CTL simulations for 10 m wind mean intensity - horizontal components - and accumulated precipitation, February 20 th	17
4.12	Taylor diagrams for horizontal wind components	17
4.13	Combined errors for wind components.	18
4.14	Taylor diagram and combined errors chart for precipitation.	19
4.15	u and v components combined errors chart for the stations located at an altitude greater than 800 m (mountainous region).	20
4.16	u and v components combined errors chart for the stations located at an altitude lower than 800 m (shore region).	20
4.17	u and v components combined errors chart for the windward region.	20
4.18	u and v components combined errors chart for the leeward region.	21
4.19	Precipitation combined errors chart for the stations located in mountainous 4.19a and shore regions 4.19b.	21
4.20	Precipitation combined errors chart for the stations located windward 4.20a and leeward 4.20b regions.	22
4.21	Taylor diagram and combined errors chart for the different microphysics schemes with respect the modelled precipitation and observed data.	23
6.1	Land use categories for the default WRF configuration (USGS) and for the CORINE land use dataset	28

6.2	Study area map showing the Lisbon region location in the Iberian Peninsula, Maps from googlemaps.com.	28
6.3	Synoptic situation for July 29 th at 12:00 UTC (ERA Interim, daily fields)	29
6.4	Three nested model domains used in WRF.	29
6.5	Location of the weather stations over Lisbon Region (blue and red dot and the location of the cross section used in this work (yellow line).	32
7.1	Time series for two meters high air temperature ($^{\circ} C$) in red and wind intensity ($m \cdot s^{-1}$) in blue for Gago Coutinho station.	33
7.2	Vertical cross section for the perturbations of the vertical wind component (shaded $m \cdot s^{-1}$) and potential temperature ($^{\circ} C$) contours (7.2a) and Turbulence Kinetic Energy ($m^2 \cdot s^{-2}$) (7.2b) in July 29 th at 13:00 UTC CTL34 simulation.	34
7.3	Vertical cross section for the pressure correlation term ($m^2 \cdot s^{-2}$) for July 29 th at 13:00 UTC CTL34 simulation.	35
7.4	Urban land use category location, on (a) control simulations and (b) UCMs simulations.	36
7.5	2-m mean air temperature ($^{\circ} C$) for (a) CTL34 Simulation, (b) difference between SLUCM and CTL33 simulations and (c) difference between BEP and CTL34 simulation during the first sub-period - July 29 th and 30 th	36
7.6	10-m mean wind speed and direction ($m \cdot s^{-1}$) for (a) CTL34 Simulation, b the difference between SLUCM simulations and c the difference between BEP simulation during the second sub-period - August 1 st and 2 nd	37
7.7	Cross section (South-North) for the day time mean TKE ($m \cdot s^{-2}$) for (a) CTL34 simulation, (b) the difference between SLUCM simulation and (c) the difference between BEP simulation for all simulated period.	38
7.8	Cross section (South-North) for (a) the vertical wind component perturbation ($m \cdot s^{-1}$) (shaded) for CTL34 simulation and difference between SLUCM (red line) and between BEP (blue line), (b) the difference between SLUCM and CTL33 simulations and (c) the difference between BEP and CTL34 simulations, for July 29 th at 13:00 UTC.	39
7.9	Cross section (South-North) for the pressure correlation term of the TKE budget equation difference ($m^2 \cdot s^{-2}$), (a) between SLUCM and CTL33 simulation and (b) between BEP and CTL34 simulation, July 29 th at 13:00 UTC.	40
7.10	Taylor diagram and combined errors chart for temperature for all the simulated period.	41
7.11	Taylor diagram for (a) u and, (b) v wind components and combined error chart for (c) u and (d) v wind components for all the simulated period.	42
7.12	Taylor diagram and combined errors chart for temperature profile taken from radiosonde data for all the simulated period.	42
7.13	Time series of PBL height for observed data and it respective standard deviation (red) and for CTL34 (grey), CTL33 (blue), SLUCM (orange) and BEP (green) simulation.	43

List of Tables

3.1	Topography and land use data set attributes.	7
3.2	Lower boundary conditions and microphysics schemes used on WRF simulations. . . .	7
3.3	Weather Station information used to evaluate model skill.	8
6.1	Description of the WRF UCMs features - Table adapted from Wyszogrodzki et al. (2012).	30
6.2	Description of the WRF UCMs information introduced in the PBL scheme - Table adapted from Wyszogrodzki et al. (2012).	30
6.3	Recategorization process used to convert the eleven urban CORINE into the three USGS urban classes used by WRF UCMs.	31
6.4	Resume of the principal parameters used to describe Lisbon metropolitan area geometry in the WRF/UCM model.	31
6.5	Weather Stations information used to evaluate model skill.	32

Chapter 1

Introduction

Between the Earth's surface and the free atmosphere, there is an atmospheric layer in which the flow is strongly influenced by its interaction with the surface, leading to a continuous exchange of matter, energy and momentum, making them dependent on each other (Stull, 1988; Xue et al., 1996). Therefore it is necessary to consider the Earth's surface and the atmosphere as part of the same physical system. The time span of these interactions is generally less than an hour making it so that the atmospheric layer where they occur is characterised by rapid fluctuations of physical quantities such as flow velocity, temperature and water vapour. This turbulent layer of the atmosphere is called the planetary boundary layer (PBL).

The importance of topography in atmosphere dynamics is well known due to its influence on the sinusoidal pattern of the wind and its implications on the potential vorticity adjustments (Holton, 2004).

Numerical atmospheric models are known to be very sensitive to surface elements. In particular, many authors have shown the direct influence of topography in atmospheric properties. Pointing few examples related with the present work, Bond and Stabeno (1998), Colle and Mass (1998) and Koletsis et al. (2010) have studied the significance of an orographic wind flow through a major gap between two high mountains and concluded that the varying elevations inside an elevated gap play an important role in the gap winds intensity and flow paths. Also, it has been shown that topography influences water vapour transport and thus it can modify precipitation patterns (Jiang, 2003).

Due to the difficulty of simulating precipitation events in regions with complex topography and its eventual role as natural hazard, orographic driven precipitation has been the focus of several studies (Elementi et al., 2005; Ghafarian et al., 2012). It is also known that changes in land use can lead to changes in atmospheric properties such as local circulation, moisture and radiation balance (Bischoff-Gauß et al., 2006; Tomassetti et al., 2003). On the other hand, Viterbo and Betts (1999) have examined the impact of soil water in precipitation using different initial soil water fields. Also, Weigel et al. (2007) have shown how the moisture fluxes can alter moisture exchange between the surface and the free atmosphere.

Given the close relationship between the surface and the atmosphere, it is evident that Earth's surface properties take an important role in atmospheric dynamics. Therefore the best knowledge on surface parameters is important to atmospheric studies and research specially when dealing with numerical atmospheric models where small perturbations can propagate throughout the whole atmosphere.

Through the years, the advances in satellite technology made feasible the acquisition of information about the Earth surface, such as elevation and land use, with great detail and resolution. Using this information it is possible to obtain lower boundary conditions that can be used in numerical atmospheric models, allowing the models to better represent the local surface characteristics. This is especially important for regions with a complex topography, where the surface elevation is roughly represented with low resolution information and mixed land use, where soil properties may influence the heat fluxes at this lower boundary.

Among several projects that have treated the raw data imagery there is the Shuttle Radar and Topography Mission (SRTM), the ASTER Global Digital Elevation Model (ASTER) and the Coordination of Information on the Environment Land Cover (CORINE). The former is a joint project between National Aeronautics and Space Administration and the Department of Defense's National Geospatial-Intelligence Agency, being distributed by the U.S. Geological Survey at a three arc-second resolution. This project aimed to obtain elevation data on a near-global scale to generate the most complete high-resolution digital topographic database of Earth. SRTM consisted of a specially modified radar system that flew on board the Space Shuttle Endeavour collecting data with the interferometry method (Farr et al., 2007). ASTER is a joint product developed by the Ministry of Economy, Trade,

and Industry (METI) of Japan and the United States National Aeronautics and Space Administration (NASA). It is generated from data collected from the Advanced Spaceborne Thermal Emission and Reflection Radiometer (ASTER), a spaceborne earth observing optical instrument (Tachikawa et al., 2011). The last dataset is the land use data collection from satellite image, produced by the European Environment Agency and its members, for 38 European countries with 44 land use classes of the 3-level CORINE nomenclature, with the objective of providing quantitative data on land cover, consistent and comparable across Europe. The latest update is from the year 2006 and is distributed with a 100 meters resolution (Bossard et al., 2000). These data sets can be used as lower boundary conditions in numeric atmospheric models, enabling them to be configured to run with higher spatial resolution permitting them to be up to date.

Many studies have been conducted in order to evaluate the sensitivity of numerical atmospheric models to high spatial resolution, namely the work developed by Elementi et al. (2005). This work concluded that overall precipitation was well simulated by using a seven kilometre resolution simulation albeit its spatial distribution was poorly represented. When the resolution was increased to two kilometres the precipitation patterns were better simulated. However, fewer studies can be found that evaluate the sensitivity of numerical atmospheric models to different datasets of lower boundary conditions such as topography and land use.

Along with lower boundary datasets there are model physics parametrisations that may also influence model performances at high resolutions. Microphysics may in turn be important during weather patterns associated with precipitation whereas for atmospheric high stability is most sensitive to lower boundary data and urban parametrisations.

The main objectives of the present work is to study the Weather Research and Forecast model (WRF) sensitivity to lower boundary conditions, topography and land use as well as for urban parametrisations under two types of weather patterns above cited. The first part focuses on WRF sensitivity to the two lower boundary conditions, as well as, the sensitivity to two microphysics parametrizations in an extreme orographic precipitation case in Madeira, Portugal. The second part is centred on the WRF model sensitivity to the two different urban model parametrisation and study the urban effects in the atmosphere for a period with atmospheric conditions favourable to the development of a large urban heat island over the Lisbon region.

Part I

Model Sensitivity to Lower Boundary Conditions and Microphysics.

Weather precipitation event

Chapter 2

State of The Art

As referenced before, topography plays an important role in atmospheric dynamics as it can force flow dynamics, precipitation patterns and change atmospheric water vapour concentration. Given this, the influence of topography on water vapour transport and the different forcing mechanisms, acting on different time and length scales, that can produce orographic precipitation has been the focus of several studies for the past decades.

Due to the complexity of topographic forced mechanisms, studies concerning idealized situation such as an uniformly stratified moist flow over a Gaussian-shaped circular mountain, have been performed by several authors, namely by Jiang (2003); Colle (2004); Kunz and Kottmeier (2006a). The three of these works perform sensitivity studies in order to determine the relationship between the mountain's dimension and the precipitation intensity and distribution.

Under these assumptions and using a mesoscale model, Jiang (2003) as well as Colle (2004) studied the interaction between flow stagnation and orographic precipitation. In their work the authors showed that there is a significant relationship between the flow blocking and splitting effect and precipitation distribution and intensity. For low mountains the upslope ascent is dominant and the precipitation intensity is proportional to the mountain height and wind speed. On the other hand for high mountains the flow tends to pass around the barrier, reducing the lift effect. This reduces the precipitation amounts in the peaks and enlarges the area where precipitation occurs, forming an arc-shaped precipitation band further upstream of the peak where the terrain slope is smaller. In addition, the authors showed that latent heat release interacts with flow splitting and gravity wave-breaking which in turn affects precipitation distribution. Furthermore, Colle (2004) and Kunz and Kottmeier (2006a) have conducted sensitivity experiments to assess how ambient conditions and model parameters influence orographic driven precipitation. It was concluded that precipitation intensity and distribution present a significant sensitivity to ambient conditions such as static stability, surface temperature, wind speed and vertical shear. With regard to model parameters, Kunz and Kottmeier (2006a) showed that the results are less sensitive to model parametrizations than to ambient conditions. Although precipitation can be affected by the bulk microphysics parametrizations, specially on the lee side of the mountain, Colle (2004) showed that they have no effect on the fundamental changes in orographic cloud and precipitation structures. Later, Kunz and Kottmeier (2006a) applied the formulation used in their idealised model to a real case study, for which model simulated precipitation was found in good agreement with observations in both magnitude and location (Kunz and Kottmeier, 2006b).

In addition to idealized studies, abundant real case studies have been performed concerning the effect of mountain barriers in climate, interaction with synoptic scale processes or even studies of single cases of extreme orographic precipitation. Atmospheric numerical models have been found to be useful in order to assess precipitation in areas where observations are scarce and estimates are difficult (Maussion et al., 2010). In order to study precipitation patterns in the Tibetan Plateau, Maussion et al. (2010) used the WRF model and conducted a one month model validation against observed data. In their work the authors concluded that the numerical model showed good accuracy in simulating precipitation. As Vrochidou and Tsanis (2012) showed in a multi year study, the precipitation patterns found in the Crete Island (Greece) have a strong correlation with the island topography. This connection was found to be an important clue for spatial drought patterns. Concerning the synoptic scale interaction, Ghafarian et al. (2012) studied the effects of the Anatolian and Caucasus mountains on the precipitation distribution over the Black Sea. For their research the authors performed the numerical simulation of a precipitating synoptic system passing through the study area. Using two different configurations, one with all the topographic features and the other in which the mountains were removed. Analysing the results Ghafarian et al. (2012) concluded that although there was a significant change in the fields of vertical motion, relative vorticity, humidity, low level geopotential height, cloud water content and precipitation distribution, the mountains were not responsible for the cyclogenesis.

Considering that topography plays an important role in flow and precipitation patterns, Shi et al. (2008) conducted a topography sensitivity study, for the Tibetan Plateau. In one simulation the authors used a topography resolution consistent with the numerical model spatial resolution (30 km) and in the other, a 120 km resolution topography that was then interpolated in order to be consistent with the model was used, generating smoothed topographic features. Model results showed that the simulation with higher resolution topography agreed with the observed precipitation. On the other hand, the simulation that used the coarser resolution, considerably underestimates the observed precipitation. Besides the effects of topography changes in flow and precipitation patterns Chen et al. (2001) showed how lower boundary conditions, for example soil moisture and land use, may affect precipitation and convection in a flash flood case study. Couto et al. (2012) identified and studied four cases of intense precipitation over Madeira Island during the winter of 2009/2010 using both observed and simulated data. In their work the authors concluded that Madeira's orography is the dominant factor both in the formation and intensification of precipitation, being the altitude the main factor contributing to the precipitation distribution.

In the study presented here, a mesoscale numerical weather prediction model was used to assess the sensitivity of the model to a precipitation extreme event. The chosen event occurred on the morning of the 20th of February, 2010 over the Madeira Island. This event was associated to a frontal system, embedded in a depression centred over the Azores archipelago, and moving to the northeast. The occurred precipitation intensity triggered flash floods and mudslides, which had important social and economic consequences. Over 40 people died in the event and several houses and structures were damaged or destroyed.

Previous work had already studied the ability of numerical models to forecast this extreme precipitation event, namely Grumm (2010) who analyzed the ability of the National Center for Environmental Prediction of the United States of America ensemble Global Forecasting System (GFS) to forecast this event and concluded that the pattern associated to the heavy precipitation event over Madeira was well predicted. Also Luna et al. (2011) found that orography was the main factor explaining the precipitation event's amplitude and phase over the island. Furthermore, it was shown in this work that horizontal resolution is an important factor when simulating local precipitation.

Chapter 3

Method and Data

The numerical model used in this work is the Weather Research and Forecasting Advance Research model (WRF-ARW) version 3.3 (Skamarock et al., 2008). Initial and lateral boundary conditions from GFS analyses (NCEP, 2003) were provided to the model at a three hour interval. The GFS model has an approximated horizontal resolution of $0.5^\circ \times 0.5^\circ$ that extends vertically from the 1000 to 0.27 hPa in 64 unequally spaced model levels.

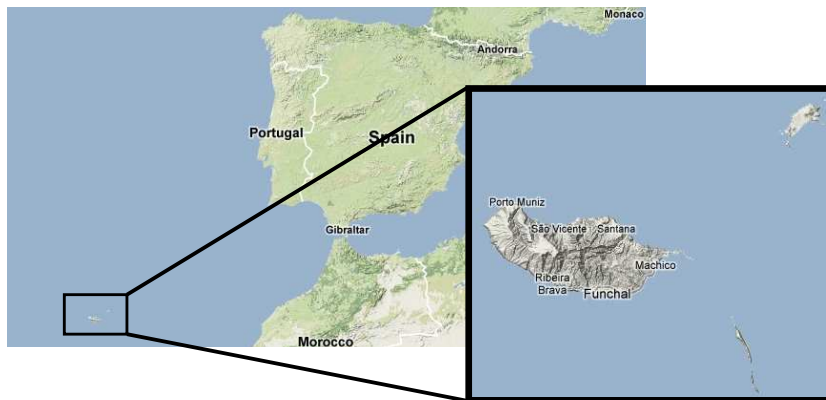


Figure 3.1: Study area map showing the Madeira archipelago location in the Atlantic Ocean, Maps from googlemaps.com.

The Madeira Island is located in the Atlantic Ocean South-west of mainland Portugal - Figure 3.1. It has a mountain ridge extending along the central part of the island reaching a maximum altitude of 1862 m - Pico Ruivo.

Three two-way nested domains were applied to the study area - Figure 3.2. The parent domain (d01) with horizontal resolution of 25 km, and two nest domains (d02 and d03) with an horizontal resolution of 5 and 1 km, respectively. The simulated period was 24 hours, starting on February 20th, 2010.

Ferreira (2007) compared several sets of physical parametrizations used in the WRF model for mainland Portugal. To find out the best combination of parametrizations model results were compared with observed data. The set of parametrizations which were found to give the best results were used in the present study. Therefore, the following schemes were used: WRF Single-Moment 6-class scheme microphysics (Hong and Lim, 2006), Goddard shortwave radiation (M.D. and Suarez, 2001), Rapid Radiative Transfer Model (RRTM) longwave radiation model (Mlawer et al., 1997), the Eta similarity surface layer scheme (Janjić, 2002), Mellor-Yamada-Janjic planetary boundary layer scheme (Janjic, 1990) and the Noah Land Surface Model (Chen and Dudhia, 2001). Cumulus have been resolved explicitly as Luna et al. (2011) showing that cumulus parametrization is not relevant to simulated precipitation in this particular event.

In order to conduct sensitivity tests to the topography and land use, several experiments were performed. In these experiments two topography data sets - SRTM and ASTER GDEM - and a land use data set - CORINE - were used. A control experiment (CTL) was conducted with the WRF default topography data set - GTOPO30 - and the default land use data set - USGS global 30' vegetation data (USGS30). Some of the more relevant data set attributes are described in Table 3.1.

Due to the different classification methods used in the CORINE and the USGS global vegetation data, a recategorization was performed to the CORINE data set to be recognizable by the WRF model. The recategorization process used to convert CORINE into USGS categories is described in

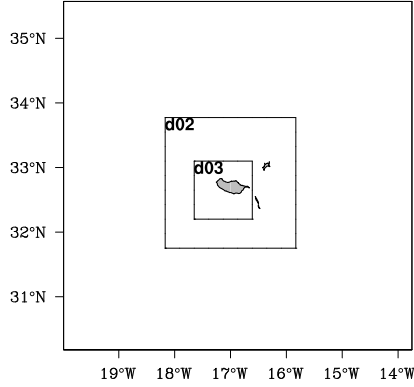


Figure 3.2: Three nested model domains used in WRF.

Table 3.1: Topography and land use data set attributes.

	Resolution	Year	Soil Categories
GTOPO30	30"	1996	NA
SRTM	3"	2005	NA
ASTER	1"	2009	NA
USGS30	30"	1993	25
CORINE	100 m	2006	44

Pineda et al. (2004).

As depicted in the previous chapter, several authors showed that model results are sensitive to microphysics parametrizations. Therefore, sensitivity tests to a set of two microphysics parametrizations suitable for high resolutions simulation were performed. The microphysics parameterizations used are described by Lin et al. (1983) and Thompson et al. (2004). The performed simulations were grouped into two sets - topography sensitivity tests (TP) and microphysics sensitivity tests (MP) - as can be seen in Table 3.2.

Even though performance analyses and validation is usually performed using state variables such as temperature and pressure, this study is focused on the Madeira extreme precipitation event and therefore only this variable together with wind will be analysed.

Table 3.2: Lower boundary conditions and microphysics schemes used on WRF simulations.

Simulation Set	Run	Lower Boundary Condition	Microphysics Scheme
Control	CTL	GTOPO30 + USGS30	Hong and Lim (2006)
TP	SRTM	SRTM + USGS30	Hong and Lim (2006)
	ASTER	ASTER + USGS30	Hong and Lim (2006)
	CORINE	GTOPO30 + CORINE	Hong and Lim (2006)
MP	MP1	GTOPO30 + USGS30	Lin et al. (1983)
	MP2	GTOPO30 + USGS30	Thompson et al. (2004)

In order to analyse model results, focusing on the evaluation of the WRF model sensitivity to topography and microphysics, the difference fields related to precipitation and wind were computed between the experiments and the control simulation. Furthermore, the study domain was divided following the mountain ridge of the island, in order to be able to study the effects of the upslope and downslope flows. Also, in order to study the contribution of the highest parts of the island on the sensitivity experiments and precipitation distribution the analysis was separated according to the mountain heights - lower and higher than 800 m. Finally, a more detailed study of simulated hourly precipitation and wind was done. Comparison with observed hourly precipitation and wind data as

well as skill analysis for every experiment were performed.

In their study, Luna et al. (2011) have shown that high model resolution enhances the model skill in this particular event. Therefore this work will focus in the domain with higher resolution - d03.

A total of 12 weather stations were considered, five of which are owned and operated by the Portuguese Meteorological Institute and present only precipitation data - Areeiro, Funchal, Lugar de Baixo, Ponta do Pargo and S. Jorge. The other seven stations are owned and operated by the Madeira Regional Civil Engineer Laboratory and present precipitation and two meter wind speed and direction data - Bica da Cana, Calheta, Encumeada, S. Martinho, Machico, Parque Ecológico do Funchal, Porto Moniz. For both sets of weather stations, data are available on hourly bases, for a period from 00:00 UTC 20 February 2010 to 00:00 21 February 2010. Location and altitude information about these stations are shown in Table 3.3 and Figure 3.3. Furthermore, in order to produce vertical profiles of the atmospheric properties, a meridional cross section was considered at a longitude of $16.93^\circ W$, considering all latitudes within the higher resolution domain - d03 - as can be seen in Figure 3.3.

Table 3.3: Weather Station information used to evaluate model skill.

Location	Latitude ($^\circ$)	Longitude ($^\circ$)	Altitude (m)
Lugar de Baixo	32.67	-17.08	15
Funchal	32.64	-16.89	58
Machico	32.73	-16.78	170
S. Jorge	32.83	-17.90	185
S. Martinho	32.65	-16.94	250
Ponta do Pargo	32.81	-17.26	312
Porto Muniz	32.84	-17.19	675
Encumeada	32.75	-17.02	1017
Calheta	32.77	-17.18	1020
P.E. Funchal	32.70	-16.90	1300
Bica da Cana	32.76	-17.06	1600
Areeiro	32.71	-16.91	1610



Figure 3.3: Location of the weather stations in Madeira Island (blue doted - Portuguese Meteorological Institute; White doted - Madeira Regional Civil Engineer Laboratory) and the location of the cross section used in this work (red line).

In order to analyse the model performance, some relevant measures were determined according to Pielke (2002) and also applied by Luna et al. (2011) for WRF simulation of the same precipitation event.

- Deviation of the modelled data in relation to observed values:

$$\phi'_i = \phi_i - \phi_{i,obs} \quad (3.1)$$

- Bias, which represents the mean deviation of the modelled data in relation to the observed values.

$$Bias = \frac{1}{N} \sum_{i=1}^N \phi'_i \quad (3.2)$$

- The Root Mean Square Error.

$$E = \sqrt{\frac{\sum_{i=1}^N (\phi_i - \phi_{i,obs})^2}{N}} \quad (3.3)$$

- Error Standard deviation:

$$STDE = \sqrt{\frac{1}{N} \sum_{i=1}^N \left(\phi'_i - \frac{1}{N} \sum_{i=1}^n \phi'_i \right)^2} \quad (3.4)$$

- The Root Mean Square Error after the removal of a constant bias.

$$E_{UB} = \sqrt{\frac{\sum_{i=1}^n [(\phi_i - \bar{\phi}) - (\phi_{i,obs} - \bar{\phi}_{obs})]^2}{N}} \quad (3.5)$$

- Standard deviation for the modelled - equation 3.6 - and observed data - equation 3.7.

$$S = \sqrt{\frac{\sum_{i=1}^n (\phi_i - \bar{\phi})^2}{N}} \quad (3.6)$$

$$S_{obs} = \sqrt{\frac{\sum_{i=1}^n (\phi_{i,obs} - \bar{\phi}_{obs})^2}{N}} \quad (3.7)$$

were the i is the temporal index and N is the number of elements of ϕ considered.

Given this the modelled data better reproduces the observations when the modelled standard deviation is approximated to the observed, the error from the simulations is within the natural variability of the observations and the modelled bias squared is smaller than the error squared. Considering that the model skill is high when the following criteria is verified:

- $S \approx S_{obs}$
- $E < S_{obs}$
- $E_{UB} < S_{obs}$
- $Bias^2 \ll E^2$

Chapter 4

Results and Discussion

4.1 Synoptic Setting

Throughout the period under analysis, the synoptic setting over Madeira Island - Figure 4.1 - shows a rapid transition from high to low pressure systems. Between February 19th and 20th, the surface horizontal pressure gradient was weak and, at the 500 *hPa* level the island was flanked by a trough on right and a ridge on its left side and there were two depressions located near the Labrador Sea. By February 20th, these two depressions had deepened and were moving westwards, forming a trough at mean sea level with a high on its right side. On February 21st, western flux was imposed by the advection of these low pressure systems to west. Keeping in mind that precipitation analysis is dependent on horizontal model resolution, this discussion is focused only on the third nested domain.

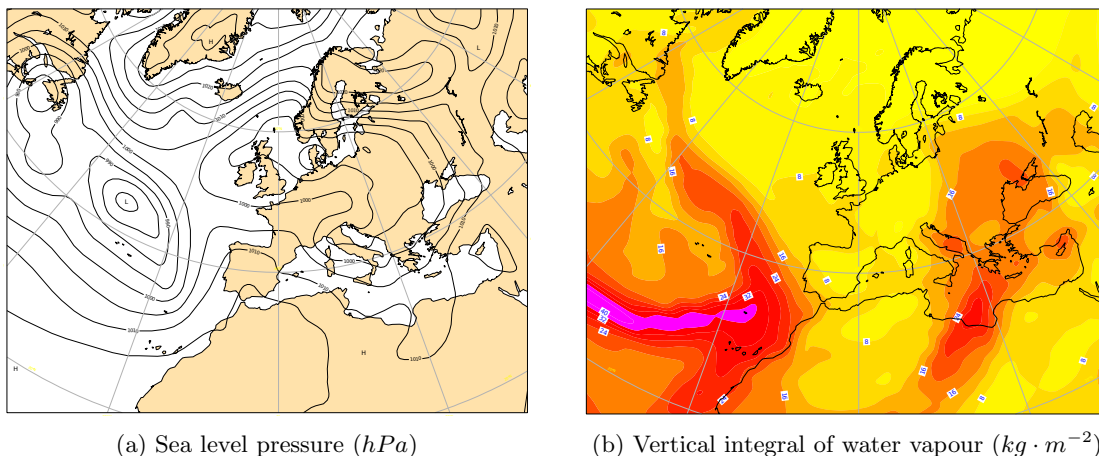


Figure 4.1: Synoptic situation for February 20th at 12:00 UTC (ERA Interim, daily fields)

When comparing the results of this study with others that evaluate the orographic influence on precipitation (idealized studies by Colle (2004) and Kunz and Kottmeier (2006a) - and real data study by Kunz and Kottmeier (2006b)), some similarities arise. Madeira Island might be regarded as a singular barrier disturbing the synoptic flow, just as in most idealized experiments. Also, during the simulated period the atmosphere is stable stratified - Figure 4.2. Therefore, an enhancement of local precipitation over the windward side of the barrier and less precipitation on their lee side due to the subsidence associated to the gravity waves is expected, as shown by Colle (2004) and Kunz and Kottmeier (2006a). The mountain crests of Madeira Island located perpendicularly to the main flow forces the air mass to rise as it climbs the windward slope on the southern side of the island, capturing moisture on the orographic induced gravity waves on the northern side. This flow dynamics and its precipitation distribution pattern was also verified and studied by Luna et al. (2011) and Couto et al. (2012).

4.2 Sensitivity to Topography

4.2.1 Topography datasets

All simulations have the same grid resolution. However, due to the different topography and land use dataset resolutions an interpolation was performed to the lower boundary data in order to have

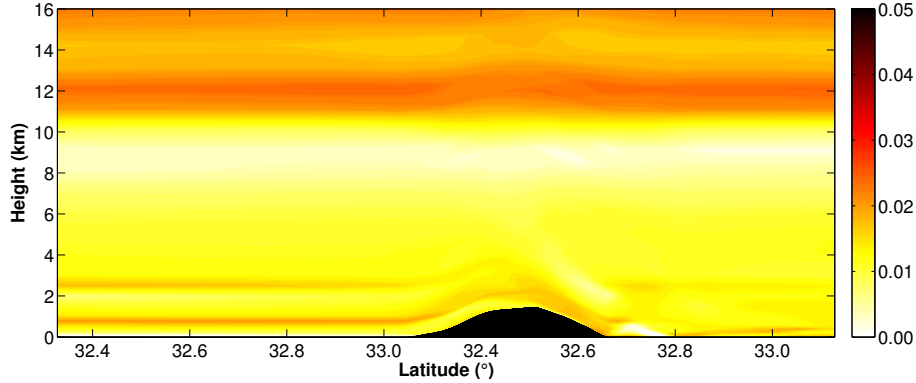


Figure 4.2: Vertical cross section for Brunt-Väisälä frequency (s^{-1}) for February 20th at 12:00 UTC control simulation.

consistency with the CTL simulation, thus permitting a direct comparison between simulations.

In figure 4.3 one can see the Madeira Island topography as was used for the CTL simulation (4.3a). Figures 4.3c and 4.3d show the difference between CTL and SRTM (SRTM - CTL) and ASTER (ASTER - CTL), respectively. In addition, the topography of the cross section used in this work for CTL, SRTM and ASTER is shown on the upper right-hand side (figure4.3b).

As can be seen, the default topography tends to represent smoother topographic features. On the other hand the high resolution data sets present a better representation of those features with higher peaks and deeper valleys as well as steeper terrain slopes. These characteristics make it a better representation of Madeira Island topography.

With regard to the SRTM and ASTER data sets, both show a similar representation of the island topography, with only slight differences between them at the top of the island and in the mid northern slope.

4.2.2 Wind modelled data

As seen before, topography driven precipitation is highly dependent on flow intensity and direction (Jiang, 2003; Colle, 2004; Kunz and Kottmeier, 2006a). Furthermore, it is known that a change in topography may lead to a change in flow characteristics.

Figure 4.4a shows the wind direction and intensity of the horizontal wind components at ten meter height for February 20th at 06H00 UTC for the CTL simulation. As can be seen, in the beginning of this day, the simulated wind flow is perpendicular to Madeira's mountainous ridge - from South - thus originating a deceleration zone upstream Madeira Island, causing flow stagnation near the shore. Its weak intensity ($\sim 10 m \cdot s^{-1}$) makes for weak wind flow splitting and therefore ascent flow is dominant. The strongest winds are reproduced by this model simulation right after the mountainous region - down slope - with an approximate intensity of $20 m \cdot s^{-1}$. Nonetheless, in the central Northern leeward side of the island there is a weak flow zone from variable directions ($< 5 m \cdot s^{-1}$), created by the presence of the mountain ridge - orographic shadow zone. This area suggests the presence of mountain wakes downwind of the higher peaks of the Madeira Island.

Later, at 12 UTC - Figure 4.4b - it is possible to observe that the wind flow becomes more intense ($\sim 20 m \cdot s^{-1}$). This flow intensification enhances the flow splitting, making flow intensity stronger near the Eastern and Western ends of Madeira Island. A proportional intensification of wind intensity after the mountainous region is also noticeable. However, it can be seen that the upwind stagnation zone deepens into the island, becoming closer the island peaks. In addition, on the central Northern leeward side of the island the weak flow zone becomes narrowest due to the flow intensification at the western and eastern island borders.

After 18 UTC the wind flow weakens and changes direction to West, becoming parallel to the Madeira Island mountainous ridge. At this time flow splitting becomes dominant due to the orientation of the wind in relation to the barrier. Therefore, despite not being shown here, a strong wind flow arise in the Southern and Northern Madeira's shore.

Throughout the day, the difference field for wind direction and intensity maintains its character-

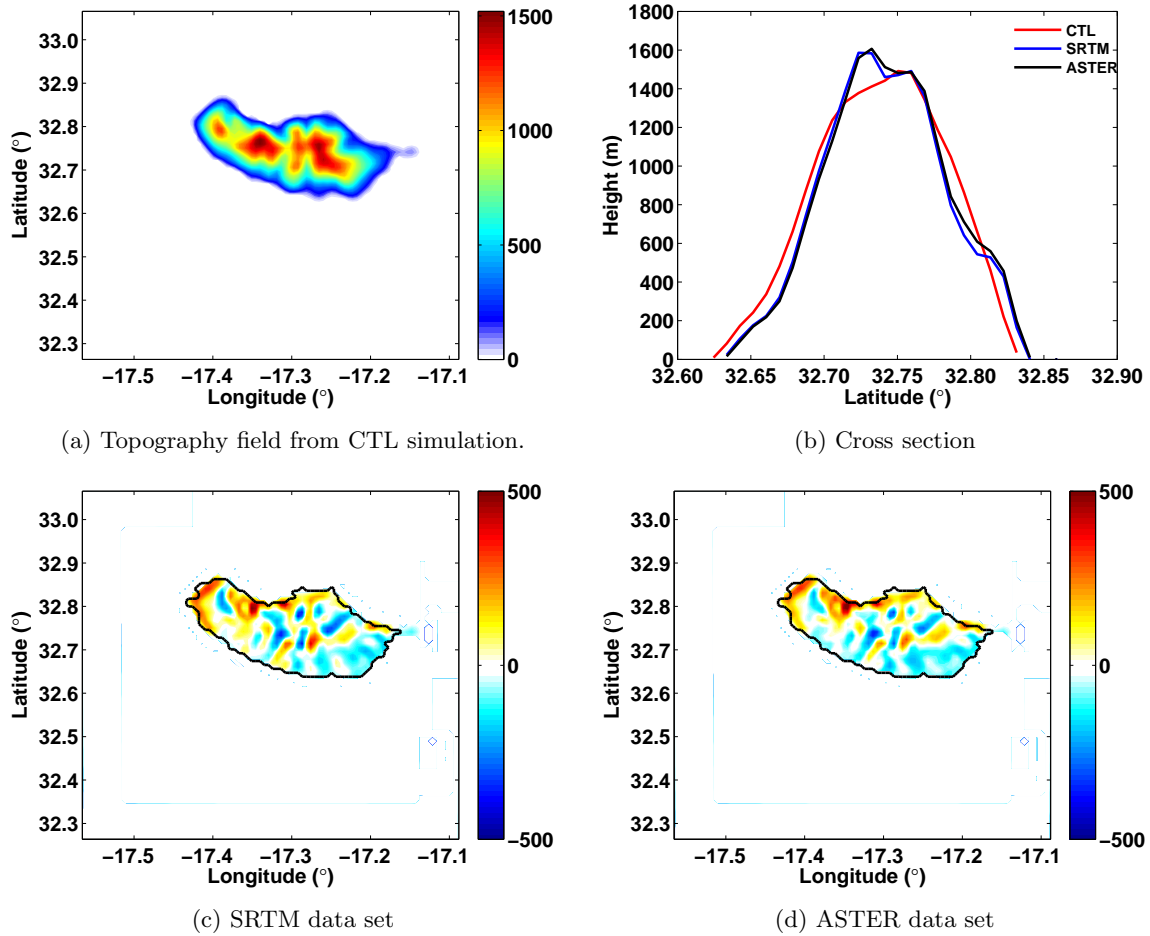


Figure 4.3: Topography field for CTL simulation (m) and topography cross section for the three data sets, CTL (red), SRTM (blue) and ASTER (black) simulations, and difference fields (m) between both high resolution topography data sets and the control topography for domain d03 at a resolution of one kilometre.

istics, with most of the differences located over Madeira Island and on its leeward side.

The difference field for intensity at a ten meter height (shaded) between SRTM and ASTER with CTL simulations and direction (SRTM and ASTER in red arrows and CTL in black arrows) for February 20th at 12 UTC are shown in Figure 4.5. Here it is possible to observe that, for both SRTM and ASTER, the differences are similar, placed in the same area and with differences in amplitude only, showing that there are no major changes in wind direction between them. It is also possible to see that greater changes are located leeward, after the wind flow passes through the Madeira mountainous crests in an area where, for CTL simulation, the wind intensity was weak, with a negative difference at the left side and a positive difference in the right side. The location of these differences may suggest that there is a displacement of the orographic shadow zone between both SRTM and ASTER simulations when compared to the CTL dataset. There is also an intensification zone - positive difference - for the high resolution topography simulations near Ponta do Pargo. This area is located in the Western end of the Island where the slope is steepest, hence, the use of the higher resolution data changes the model topography over this region of the simulated domain, as can be seen in Figure 4.3. This fact may affect the flow splitting causing acceleration in this zone.

Over land there is a number of positive and negative differences that remain stationary over time, suggesting a strong relationship to the topographic differences that may change the wind flow path. In fact, and as shown in Figure 4.6 where the difference field for mean wind intensity at a ten meter height between SRTM and ASTER with CTL simulations for February 20th is shown, it is possible to see

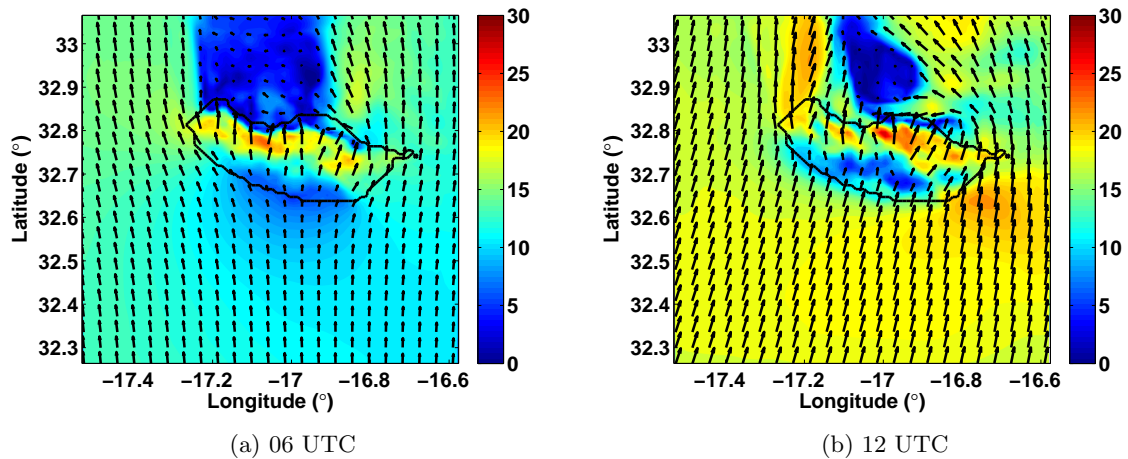


Figure 4.4: Wind direction (arrows) and intensity (shaded) ($m \cdot s^{-1}$) for the horizontal wind components at a ten meter height of February 20th at 12 UTC for the CTL simulation at 06 and 12 UTC.

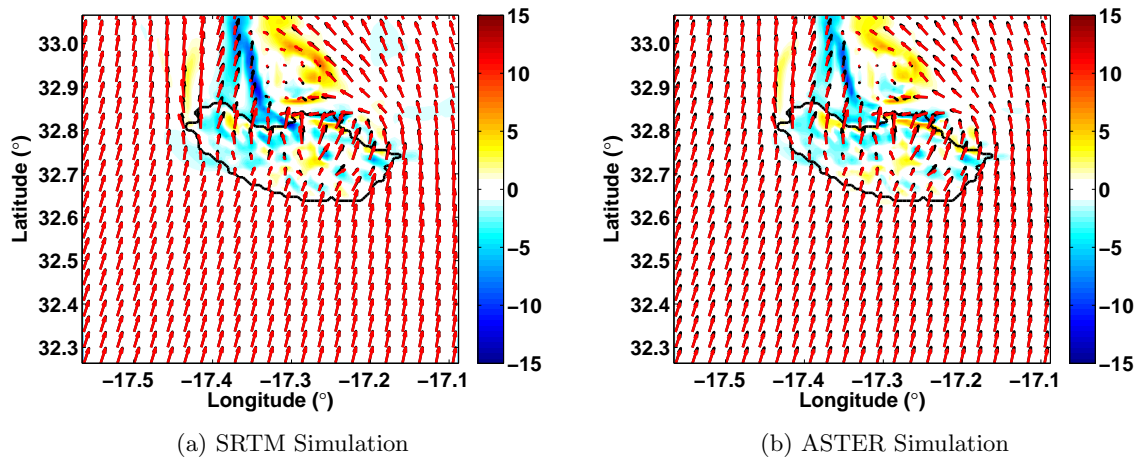


Figure 4.5: Difference field for intensity ($m \cdot s^{-1}$) at a ten meter hight (shaded) between SRTM and ASTER with CTL simulations and wind direction for SRTM and ASTER (red arrows) and CTL simulations (black arrows) for February 20th at 12 UTC.

that there are only slight differences in amplitude between the SRTM and ASTER when compared to the CTL simulation. In fact, these differences present a strong correlation coefficient when compared to their topography difference - 0.606 for SRTM simulation and 0.603 for ASTER.

4.2.3 Precipitation modelled results

As Luna et al. (2011) and Couto et al. (2012) have shown, this particular precipitation event was forced by topography flow lifting - orographic precipitation. Given the effect that a different topography dataset have in flow properties, as seen in the previous subsection, differences in precipitation distribution and intensity are also expected.

Figure 4.7 represents the accumulated precipitation for February 20th CTL simulation. Analysing this figure it is possible to observe that high amounts of precipitation occur in the centre of Madeira Island near the highest peaks. It is also possible to observe that in the southern part of the island - upstream the main flow - there is a large amount of simulated accumulated precipitation as would be expected. As it encounters the barrier - Madeira Island - the air is forced to rise. The raising moist air cools and creates favourable conditions for precipitation to occur. On the other side of the island

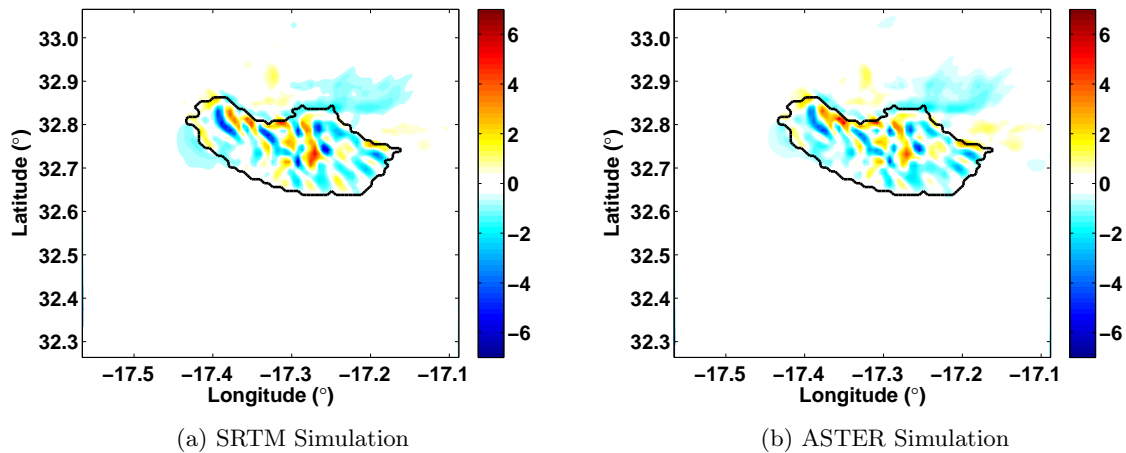


Figure 4.6: Difference field for mean wind intensity ($m \cdot s^{-1}$) at a ten meter height between SRTM and ASTER with CTL simulations for February 20th.

- the Northern part - there is a decrease in precipitation due to air subsidence and lower moisture content. Therefore, the simulated accumulated precipitation amounts are reduced in this area. This precipitation distribution and patterns are consistent with those that Luna et al. (2011) and Couto et al. (2012) have described for this particular precipitation event.

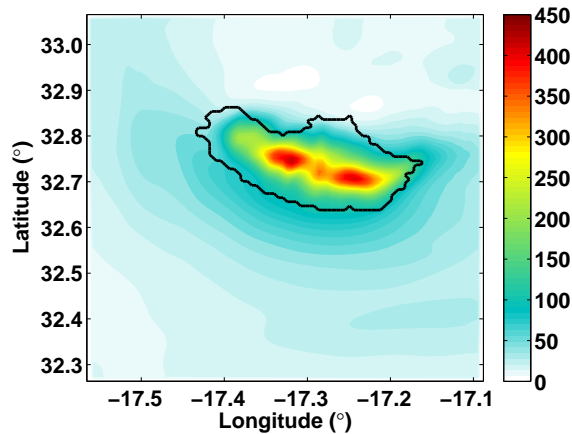


Figure 4.7: Accumulated precipitation ($mm \cdot day^{-1}$) for February 20th in domain d03 for control simulation.

When comparing the results of SRTM and ASTER simulations with the CTL it is evident that differences occur over the island. In Figure 4.8 the accumulated precipitation difference fields between both SRTM and ASTER and the CTL (SRTM - CTL and ASTER - CTL) simulation for February 20th are shown. In this figure it is possible to see that the pattern of the difference field is similar for both simulation in amplitude and in distribution. Furthermore, it is evident that in the Western part of Madeira Island most of the differences are positive, which shows that there is an increase in simulated precipitation for these simulations. This region of the island is characterised by a steep slope followed by a plateau at an height of 1400 m that is oriented perpendicular to the main flow. As seen before, SRTM and ASTER simulation have a more detailed topography and, therefore, there is an increase of the terrain slope adjacent to the plateau. Consequently it is plausible that steeper slopes enhances the terrain forcing leading to a stronger air rise that may then lead to an enhancement of topographic driven precipitation.

Centred in Madeira Island, it is possible to observe an high negative value of accumulated precipitation difference for both simulations. This negative isolated difference is associated to a deep

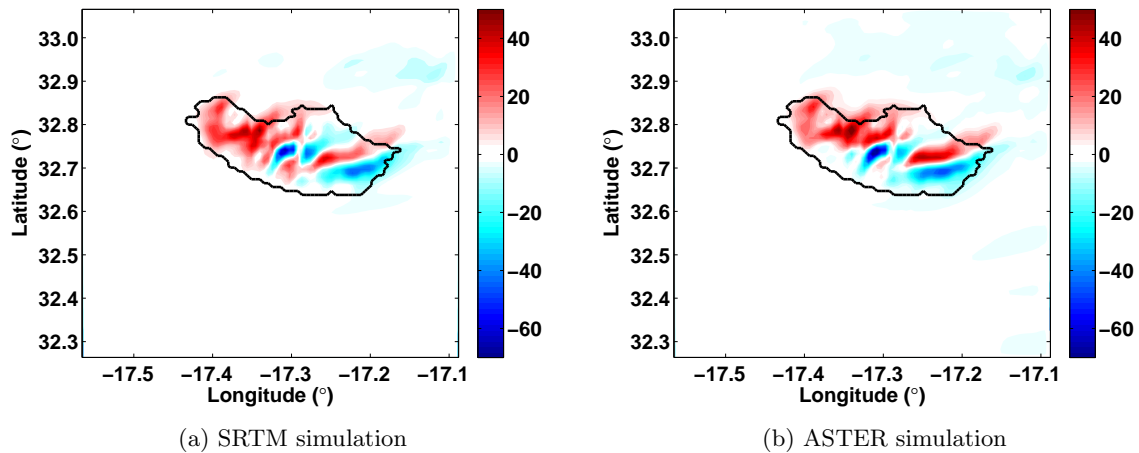


Figure 4.8: Difference fields for accumulated precipitation ($mm \cdot day^{-1}$) between both - SRTM and ASTER simulations - and the CTL simulation for February 20th.

valley - *Ribeira Brava* - located near Lugar de Baixo weather station and that extends to the top of Madeira Island. The obtained result in this area is consistent with the expected one. As the new high resolution topography data sets tend to deepen the valleys, the area of terrain forcing the air to rise is reduced which may result in a decrease in precipitation.

The highest peaks of Madeira Island are located in its Eastern region. However, near the eastern shore the slopes are not as steep as in the Western region of the island. When applying the high resolution topography it results in a decrease in precipitation near Madeira shore - negative values of accumulated precipitation difference - and an enhancement of precipitation in the Eastern mountainous regions - positive values of accumulated precipitation difference.

In addition, the correlation between the accumulated precipitation difference and the topography difference for both SRTM and ASTER was calculated with values of 0.36 and 0.46 respectively. These values, albeit small (< 0.5), show a relation between the change in topography and the precipitation difference distribution.

4.3 Sensitivity to Land Use

As mentioned before, despite all simulations having the same resolution, the use of different datasets introduces differences in the modelled results. Contrary to topography, land use changes over time scale typical of human activity and, therefore, land use datasets may change significantly every time they are updated. In addition, it must be kept in mind that there is a 13 year time gap between the USGS and CORINE land use used in this work.

In Figures 4.9 and 4.10 the USGS land use categories field for CTL and CORINE simulations are shown. It is possible to observe that there are differences in Madeira's coastline representation between CTL and CORINE simulations. In fact, CORINE dataset gives a more approximated coastline representation of the Madeira Island geographic features to the numerical model. Furthermore, significant differences in land use categories can be distinguished. For example, contrary to CTL simulation, urban and build-up land category is recognized by the model when CORINE dataset is used. Nonetheless, the area occupied by evergreen broadleaf and dryland cropland is reduced when the CORINE dataset is used. Also an increase of the area occupied by mixed forest and grassland can be observed. These changes between CTL and CORINE simulation may lead to changes in wind flow proprieties, due to changes in soil roughness length and in precipitation patterns (Chen et al., 2001).

Figure 4.11 shows the difference field between CORINE and CTL simulations for both 10-m wind mean intensity - Figure 4.11a - and accumulated precipitation - Figure 4.11b. As can be seen, the differences produced by the use of the CORINE land use dataset for this particular precipitation event are small when compared to those produced by the use of a high resolution topography dataset. For

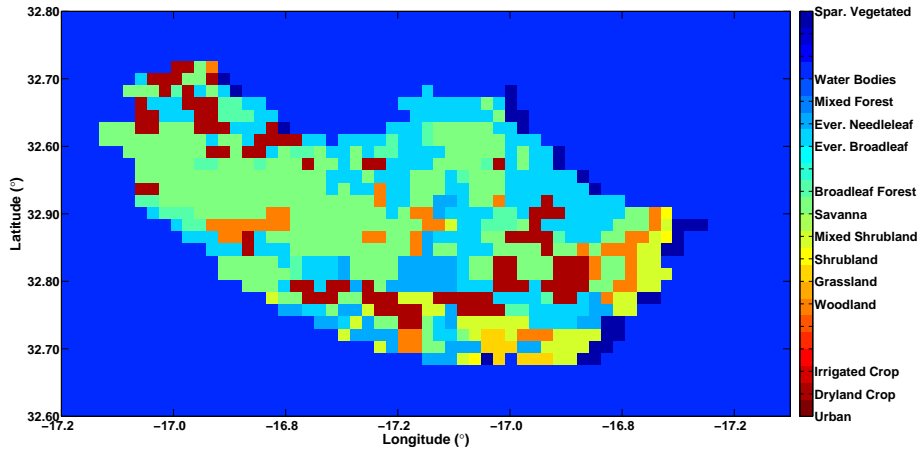


Figure 4.9: USGS land use categories field used on the CTL simulation.

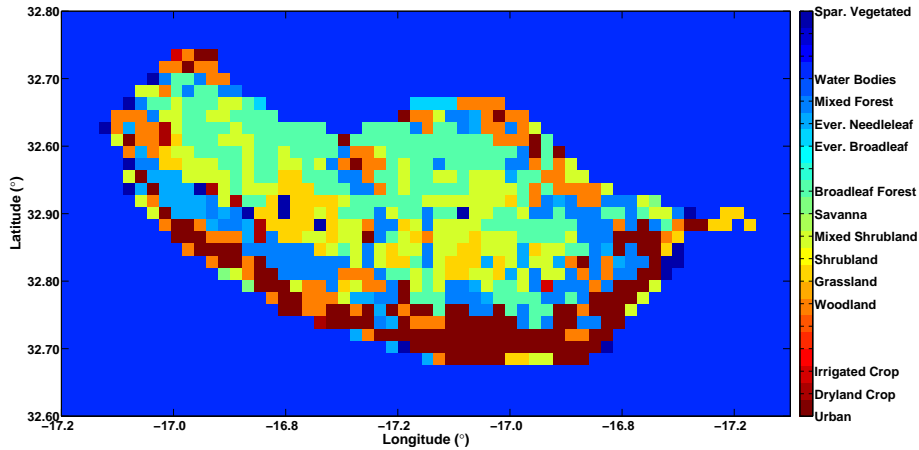


Figure 4.10: USGS land use categories field based on the CORINE land use dataset.

mean horizontal wind component intensity, it is possible to observe that in CORINE simulation there is a decrease of wind speed ($\sim 2 \text{ m/s}$) around Madeira Island shore, especially in the Eastern end of the island, where a significant change from shrubland and cropland to urban and mixed forest occurs. On the other hand, an increase of mean wind intensity in the mountainous region of the island can be observed ($\sim 2 \text{ m/s}$). When analysing the area where this wind intensification occurs - Figures 4.9 and 4.10 - it is possible to see that a change from an area characterized by the existence of deciduous broadleaf forest in CTL simulation is mostly changed to shrubland and grassland which have a lower roughness length in CORINE, thus reducing surface wind drag over this area (Chen and Dudhia, 2001).

In Figure 4.11b, where the difference field for accumulated precipitation is shown, it can be observed that their amplitude is smaller than those previously seen caused by the topography. Also it is possible to see that most differences are located only upwind Madeira Island with positive differences near Madeira's shore in an area of high density of urban and build-up land in CORINE simulation, and negative differences in the mountainous region.

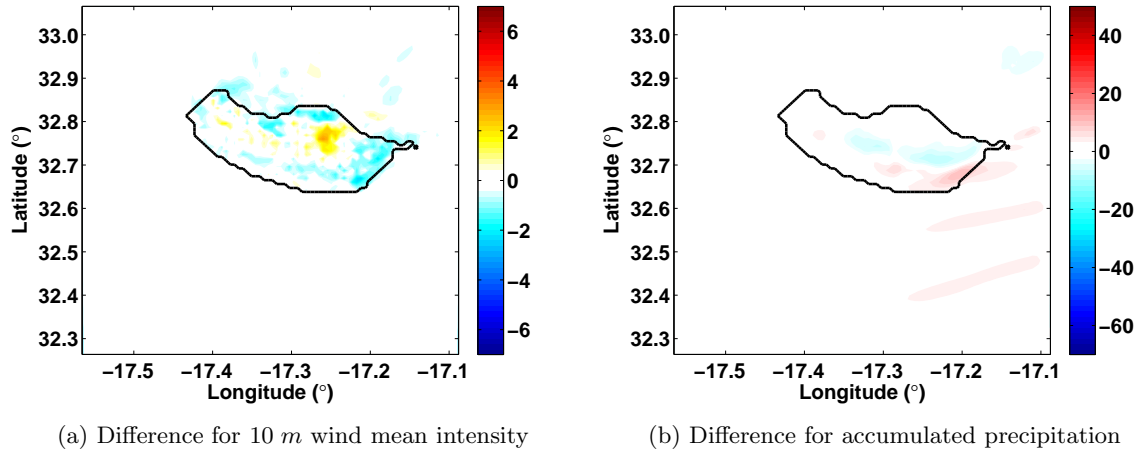


Figure 4.11: Difference fields between CORINE and CTL simulations for 10 *m* wind mean intensity - horizontal components - and accumulated precipitation, February 20th.

4.4 Modelled results vs Observed data

The previous analysis of the model results showed that, in this case study, changing to a high resolution dataset leads to a change in model results for precipitation, and wind direction and intensity. However, in order to know which one better represents the atmospheric conditions that were present throughout February 20th, the comparison of modelled data with observed data its crucial. Therefore, the analyses of simple and combined errors between the model simulations and observed data was performed.

Represented in Figure 4.12 are the Taylor diagrams for both *u* and *v* wind component. These diagrams show the standard deviations, Root Mean Square Errors and correlation between the modelled simulations' results and the observed data of all available stations where wind data were available. It is possible to see that for the *u* wind component the differences between the simulations are small. With the use of high resolution topography dataset there is a slight increase of correlation and standard deviation when comparing to the CTL simulation results. However, RMSE deviation present little change for this wind component. On the other hand, for CORINE simulation there is a minor increase of the RMSE and standard deviation and a negligible increase of the correlation.

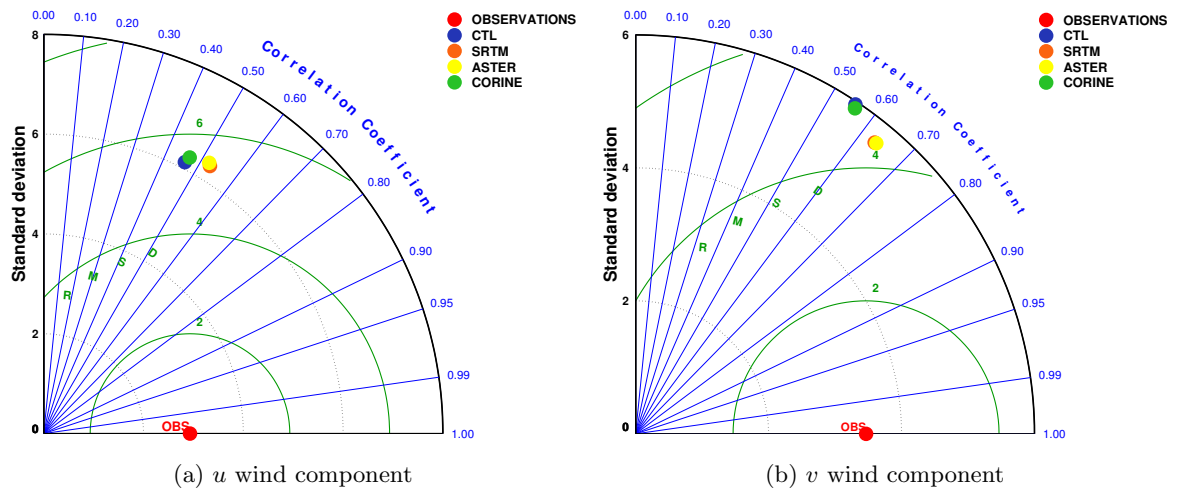


Figure 4.12: Taylor diagrams for horizontal wind components .

On the contrary, for the *v* wind component, it is possible to observe in Figure 4.12b that there is an increase of the correlation for SRTM and ASTER simulations when compared to the CTL simulation

- from 0.55 to 0.64. For the CORINE simulation changes in the statistical properties, do not present significant change when compared to CTL.

These results suggest that for all simulations the u wind component have a greater variability throughout the day, which its not present in the observed data, poorly reproducing this wind component intensity and phase as shown by its standard deviation, RMSE and correlation. On the other hand for the v wind component the increase of the correlation for SRTM and ASTER when compared to the CTL simulation suggest that for this component the use of the high resolution topography dataset enhances model skill to reproduce the observed v wind component phase. However little contribution to amplitude is verified. When comparing CORINE results with the CTL simulation it is possible to see that the RMSE, standard deviation and correlation differences are negligible for both horizontal wind components. Therefore, there is small differences in model skill to reproduce this event wind flow characteristics when using the CORINE land cover dataset.

In addition, analysing Figure 4.13 were the combined errors for both u and v wind components are shown, it is possible to see that every modelled simulation does not follow the criteria previously defined in Chapter 3 for both components, failing to adequately reproduce wind intensity - E/S_{obs} - and variability - S/S_{obs} -. Furthermore, there is a great overestimation of wind intensity by the model as can be noticed by the RMSE far higher than the standard deviation of the observed data. It can also be seen that a significant part of this overestimation may be due to inaccuracy in the specification of the initial and boundary conditions - as can be seen in the smaller EUB/S_{obs} - specially for the v wind component.

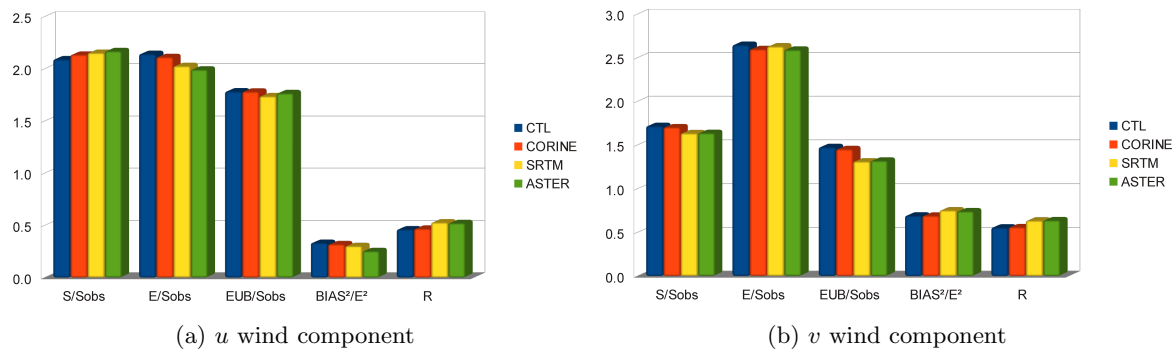


Figure 4.13: Combined errors for wind components.

However, in this analysis it must be considered that the observed wind data was taken at two-meter high and the ten-meter high wind modelled data was used in this model evaluation. Therefore, the use of vertical model levels closer to the surface can have significant impact in model results, as with this, the model is capable to better reproduce the drag due to the surface.

In Figure 4.14 the Taylor diagram - Figure 4.14a - and the combined errors chart for precipitation - Figure 4.14b - are shown. Although the model does not faithfully reproduce the observed data, it is possible to see that precipitation is modelled with skill, with most of the skill criteria being met for all the performed simulations - Figure 4.14b. Furthermore, in the Taylor diagram - Figure 4.14a - it is possible to observe that the major differences correspond to a change in standard deviation, with CTL and CORINE simulations having the closest values to the observed standard deviation and SRTM and ASTER simulations showing worse results. Nonetheless, it is possible to observe that SRTM and ASTER simulations present a slight higher RMSE. However, there is little change in correlation between the simulations and the observed data when comparing these simulation with the CTL and CORINE. Additionally, according these results, no enhancement to model skill could be seen for precipitation phase and variability, has can be observed in the values of $BIAS^2/E^2$ and for data variability. Thus, although some change to model skill is seen when simulating the wind flow with the high resolution topography datasets, there is no overall advantage in using a high resolution topography dataset when simulating precipitation for this particular extreme rainfall event.

When using a higher resolution and up to date land use information - CORINE simulation - little enhancement of model skill is detected when comparing to the CTL simulation.

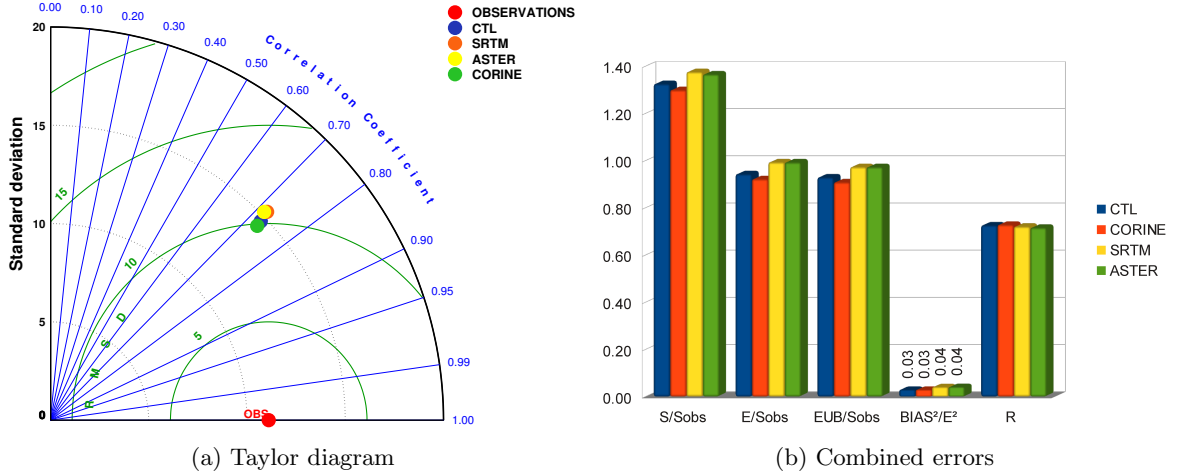


Figure 4.14: Taylor diagram and combined errors chart for precipitation.

In order to evaluate in detail the impact of using of the new lower boundary conditions datasets, Madeira Island was divided in the following regions.

- Mountainous region → Hight greater than 800 *m* five stations - Areeiro, Bica da Cana, Calheta, Encumeada and Parque Ecológico do Funchal
- Shore region → Hight less than 800 *m* seven stations - Funchal, S. Jorge, Lugar de Baixo, Ponta do Pargo, S. Martinho Machico and Porto Moniz
- Windward region nine stations - Funchal, Areeiro, Lugar de Baixo, Bica da Cana, Calheta, Encumeada, S. Martinho, Machico and Parque Ecológico do Funchal
- Leeward region three stations - S. Jorge, Ponta do Pargo and Porto Moniz)

However, for wind data analysis, fewer stations were considered since only LREC stations had wind data. Using the stations located in these regions, the study of the combined errors between the four simulations and the observations was performed for wind and precipitation data.

The combined errors chart for both *u* and *v* wind components for the Mountainous region is shown in Figure 4.15 and for the Shore region in Figure 4.16. Analysing these figures it is possible to see that results are similar to those found for the overall analysis. Considering only the mountainous region - Figure 4.15 - it is possible to observe that for both *u* and *v* wind components there is a great error in wind intensity and lag between the simulations and the observations. Nonetheless, one can see that the best results are found for the *u* wind component. In addition, for this wind component, it can be observed that albeit small, SRTM and ASTER simulations are the ones with the best skill. For the *v* wind component CTL and CORINE simulations present best performance when comparing to SRTM and ASTER.

When analysing the results for the combined error for the shore region - Figure 4.16 - it is possible to observe that, once again, better model results are found for the *u* wind component. Model skill for all the simulations performed in this region is weak. However, high resolution simulations present less amplitude and phase errors than CTL and CORINE simulations, with exception for variability. On the other hand, one can see that there is a great amplitude and phase errors in all performed simulations when simulating the *v* wind component. In addition, this error is minimized when using the high resolution datasets. However, this amplitude error reduction is insufficient to improve model skill.

Given these results, one can see that for both regions there is better model skill in simulating the *u* component than *v* wind component, which may suggest a lack of model performance for the model to simulate wind direction. Furthermore, results show greater model skill for simulating wind flow for an altitude lower than 800 *m* with some enhancement of model performance when using high topography datasets for both Mountainous and Shore regions.

Windward and Leeward regions are respectively associated with the upslope and downslope wind

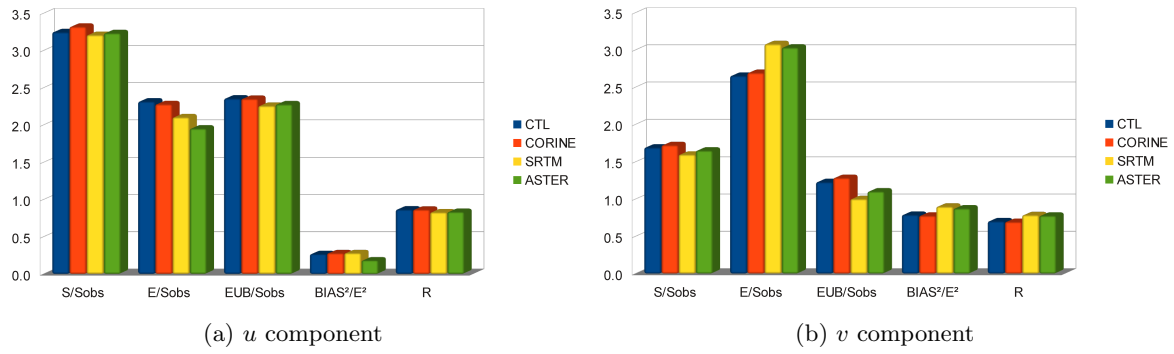


Figure 4.15: u and v components combined errors chart for the stations located at an altitude greater than 800 m (mountainous region).

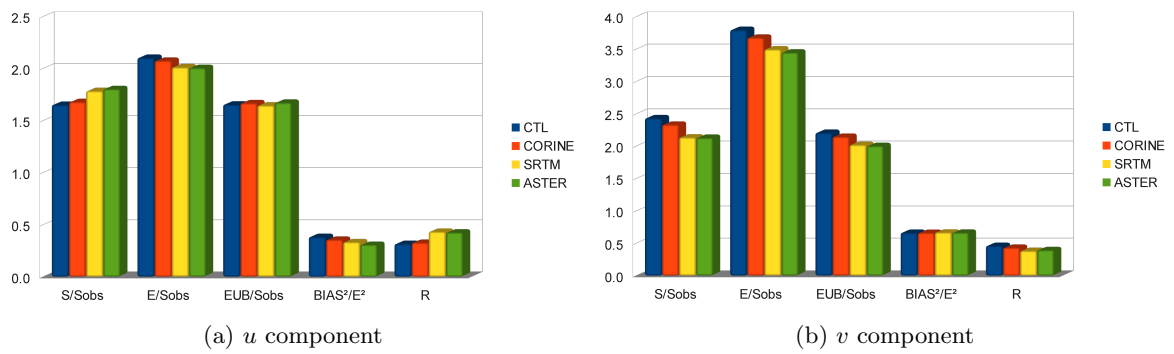


Figure 4.16: u and v components combined errors chart for the stations located at an altitude lower than 800 m (shore region).

flow. In order to better study the model skill in simulating horizontal wind flow in this regions, combined error charts were produce.

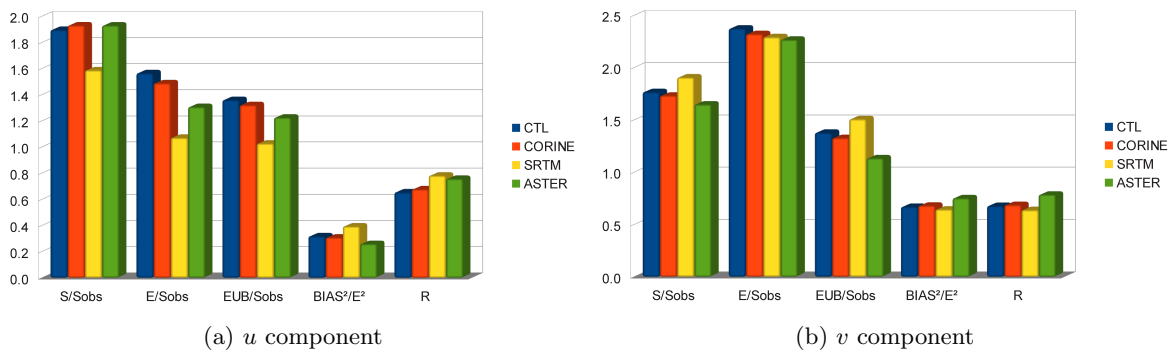


Figure 4.17: u and v components combined errors chart for the windward region.

In Figures 4.17 and 4.18 the combined error for every performed simulation for Windward and Leeward regions is shown, respectively. One can see that there is better model skill simulating u than v wind component in amplitude and phase, which may indicate errors in the simulated wind direction.

Upon a closer analysis to the combined errors for the Windward region - Figure 4.17 - in can be seen that for the u wind component there is an enhancement of model skill when using the high resolution topography datasets, specially with the SRTM dataset (Figure 4.17a). These simulations present better skill reproduction of wind flow intensity, as well as better variability and correlation. However, grater lag is produced in this simulation, as one can see by the larger $BIAS^2/E^2$ values. Just as happens for u component simulated by ASTER, v wind component does not present model

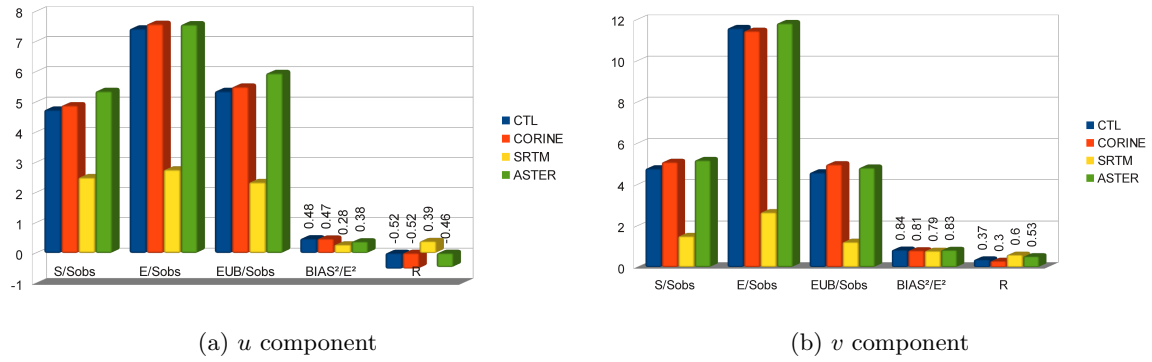


Figure 4.18: u and v components combined errors chart for the leeward region.

skill enhancement.

In the Leeward region - Figure 4.18 all simulations have a poor performance, with great amplitude and phase error, as well as a negative correlation between most simulations and the observed data. However, for SRTM simulation the amplitude and phase errors are greatly reduced when comparing with the remaining performed simulations, resulting in an enhancement of model skill. Nonetheless SRTM is the only simulation that is not anti correlated with the observations. Once more, for v wind component the same behaviour can be observed, with an enhancement of model skill when using the SRTM topography dataset. Furthermore, SRTM simulation presents a better model skill when simulating the wind in the Leeward region.

According to the results seen for Leeward region, it can be seen that using the use of SRTM topography improves model skill when simulating wind flow. However, little change was found when using high resolution lower boundary conditions datasets for the Windward region.

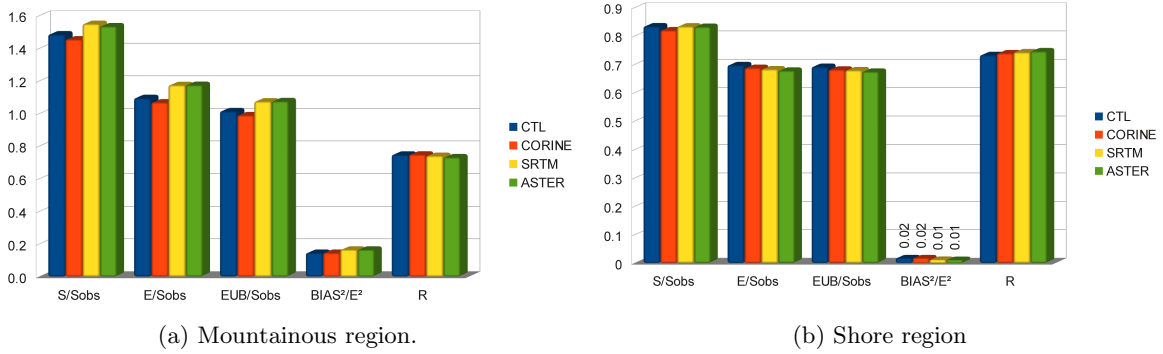


Figure 4.19: Precipitation combined errors chart for the stations located in mountainous 4.19a and shore regions 4.19b.

In Figure 4.19 the precipitation combined errors for the Mountainous region - 4.19a - and for the Shore region - 4.19b are shown. The results for the combined errors for these regions show that there is low skill when simulating precipitation in the Mountainous region with an overestimation of precipitation variability and with high amplitude and phase errors - $E/Sobs > 1$ and $BIAS^2 > E^2$. Furthermore, the use of an high resolution topography - SRTM and ASTER simulations - results in a slight decrease of model skill, not bringing any advantage to model performance when simulating precipitation in the Mountainous region. On the other hand, for the Shore region model skill is high for all simulations. Moreover, the SRTM and ASTER simulations show skill enhancement.

Analysing the precipitation combined error chart for the Windward and Leeward regions, presented in Figure 4.20b, great differences between SRTM and all the other simulations can be seen. For the Windward region - Figure 4.20a - most simulations tend to overestimate precipitation variability. Additionally, every simulation has fair model skill when simulating precipitation amplitude and phase.

However, precipitation simulated using the SRTM topography dataset have similar variability to the observed data. Also, a reduction in model error and less lag between the observations and the modelled precipitation can be observed. On the contrary, for the Leeward region 4.20b, SRTM simulation has the worst model skill, not accurately reproducing the observed precipitation amplitude and variability. All the other performed simulations present high skill simulating precipitation amplitude, underestimating the observed variability and presenting small difference between themselves.

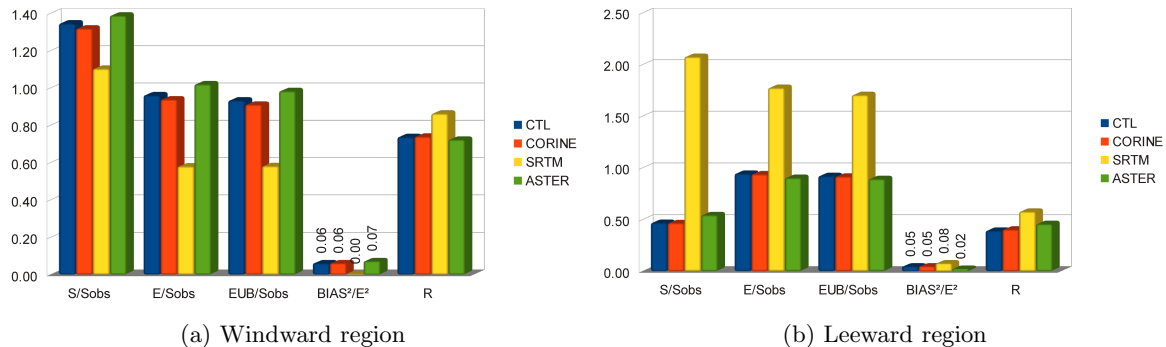


Figure 4.20: Precipitation combined errors chart for the stations located windward 4.20a and leeward 4.20b regions.

As can be seen through the analysis of these results, the use of an high resolution lower boundary condition dataset may not change model skill in most situations studied in this section. Furthermore, for some specific regions great skill enhancement can be observed when comparing to the control simulation, namely when simulating the wind on the Leeward region and precipitation on the Windward region. However, it may also decrease model skill, when using the SRTM topography dataset in the Leeward region. Nonetheless, when comparing wind results found for Leeward region - Figure 4.18 - and precipitation data - Figure 4.20b - it can be seen that the simulation with best skill for wind is the one with worst skill for precipitation. However, flow dynamics and precipitations patters in this region are highly dependent on processes occurring windward.

Considering the results presented in Figures 4.17 and 4.20a, where the combined error chart for wind and precipitation in the Windward region are shown, respectively, one can see that, as mentioned before, SRTM is the simulation that produces smallest amplitude errors, variability closet to the observed and presents the best correlation with the observed data. On the other hand, greater lag is produced for this simulation which may affect precipitation patterns in the Leeward region. Still, it can also be seen that introducing high resolution topography data to the model enhances model skill simulating wind flow in the Mountainous region and decreases skill for the Shore region. The opposite behaviour can be observed for precipitation data, with high model skill in the Shore region and similar for every performed simulation and a slight decrease of model skill when simulating precipitation in the Mountainous region, where topography is more complex.

4.5 Microphysics Sensitivity

As seen before, several authors have shown that precipitation model results are highly sensible to microphysics parametrizations. In order to assess the impact of the chosen microphysics parametrization on the simulated results in this test case, a skill comparison of three different microphysics parametrizations suitable for high resolution simulations was performed.

In Figure 4.21 the Taylor diagram - 4.21a - and the combined errors chart - 4.21b - for all the performed MP simulations for precipitation data are shown. Here, it is possible to observe that all simulations have high model skill when simulating precipitation, with a slight overestimation of precipitation variability. Furthermore, one can see that MP1 and MP2 simulations have the best overall model skill with only slight differences between them. However, the differences between these and the CTL simulations are smaller than the ones resulting from the use of a different lower boundary layer dataset, as seen in the TP simulations analysis. Therefore, the use of a different microphysics may not significantly change the results of the previous analysis.

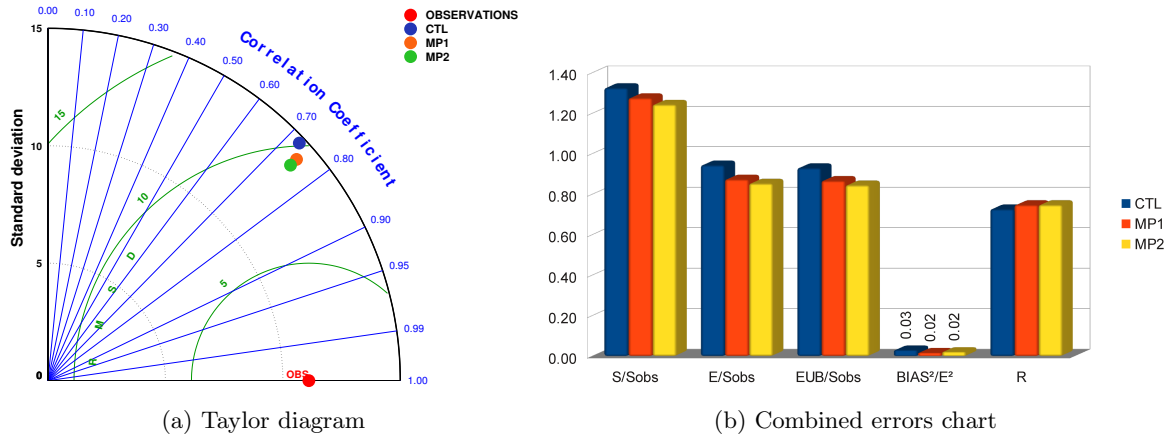


Figure 4.21: Taylor diagram and combined errors chart for the different microphysics schemes with respect to the modelled precipitation and observed data.

4.6 Synthesis

The main objective of this work is to assess the atmospheric numerical model sensitivity to lower boundary conditions. This first Part focuses on WRF sensitivity to the two lower boundary conditions in an extreme orographic precipitation event that occurred in Madeira Island, Portugal. Three high resolution lower boundary condition datasets were used to simulate this event, thereby allowing the evaluation of the sensitivity to lower boundary conditions. The datasets used were the SRTM and ASTER for topography and CORINE for land use. The simulations started at February 20th, 2010 and were extended for the following 24 hours, thus simulating all the event duration.

As mentioned in the literature, the choice of microphysics parametrisation schemes may impact model results. Therefore, in order to ascertain the sensitivity magnitude of the numerical model to these parametrizations and compare them to the sensitivity to the different lower boundary layer data, a set of simulations using three different microphysics parametrization schemes was performed. This sensitivity experiment showed that there is a little enhancement of model skill for the schemes used in MP1 and MP2 simulations for this precipitation event. This model skill enhancement may be considered negligible when compared to the one found for the sensitivity experiment to the lower boundary conditions.

Considering the default topography data used by WRF model - GTOPO30 - and the two other new topography datasets introduced in this work - SRTM and ASTER - changes can be observed in topography, albeit all simulations having the same grid resolution. With the use of the high resolution topography datasets there is a deepening of the valleys and higher peaks - changes can be greater than 100 *m* - therefore, it may better represent the topographic features of Madeira Island.

Given these differences, a comparison between the performed simulations - CTL, SRTM and ASTER - was made. There, it was possible to see that the use of any of the high resolution topography datasets may lead to changes in wind flow, specially over Madeira Island and in the leeward region. Nonetheless, it was possible to see that these changes are correlated with the differences between the topography datasets. Additionally, changes for precipitation pattern and distribution between CTL, SRTM and ASTER simulations over Madeira Island could also be observed. These changes, as seen before, are related to topographic features, as the change in terrain slope may change terrain forcing, resulting in an intensification of up lifting which may result in an increase of precipitation and vice versa. Therefore, an increase of precipitation over the mountainous ridges and a decrease of precipitation accumulated amounts over the valley, may be associated with this topographic forcing.

Comparing the simulated wind and precipitation results against observations it was possible to see that there is low model skill for *u* and *v* wind components over Madeira Island for all the performed simulations. Furthermore, when using high resolution topography datasets a slight enhancement of model skill can be observed. However, this enhancement is small. Considering the precipitation data, it could be seen that there is a high model skill. However, the observed variability for precipitation is overestimated by the model for all simulations. For this variable, SRTM and ASTER simulations

presented a decrease in model skill when compared to the control simulation. However this decrease is small.

To evaluate these changes with more detail a study considering four distinct Madeira Island regions was performed, namely Mountainous, Shore, Windward and Leeward regions. These results show, that concerning the simulation of wind flow, the model performs best for altitudes higher than 800 *m* for all the simulations. It could also be seen that, a small enhancement of model skill can be achieved for the Leeward region when using the SRTM topography dataset. For precipitation data the opposite result can be observed and there is high model skill to simulate precipitation for altitudes lower than 800 *m* for all performed simulations. Furthermore, an improvement of model skill on the Windward region can be seen when using the SRTM topography dataset. However, the use of this dataset produces more amplitude and phase errors when compared to observations for the Leeward region. For this region where all other simulations presents results that indicate a high model skill for this variable. The differences found for skill in these regions are not only caused by the use of a different topography dataset. When applying the criteria for these two regions - windward and leeward - stations located along Madeira ridge are considered to be in the different regions for SRTM, ASTER and CTL. This change may occur due to differences in the location of Madeira's ridge in the SRTM when compared to all other datasets.

Sensitivity tests were also performed with a high resolution land use dataset - CORINE. However, this dataset gives little changes to model results when compared to the control simulation.

Given this, one may conclude that the use of an high resolution dataset within WRF model leads to changes to model results for this particular orographic precipitation event. Furthermore, when comparing to observed data it can be concluded that, overall, there is no gain of model skill when using any of the high resolution lower boundary conditions datasets. However, when analysing specific regions of Madeira Island, one can see that SRTM gives an improvement of model skill on the Windward region for precipitation and on Leeward region for wind. On the other hand, decrease of model skill simulating precipitation can be observed.

Part II

Model Sensitivity to Lower Boundary Conditions and Urban Parametrizations.

High pressure weather pattern

Chapter 5

State of The Art

Technological advances turns feasible the acquisition of high resolution topography and land use data, as well as the capability of atmospheric numerical models to compute more complex physics emanating from the wide range of scales.

The classical approach used in models for coupling urban surfaces is to represent urban areas as flat surfaces with high roughness length and modified surface properties (Nadeau et al., 2009). Nowadays, mesoscale meteorological models coupled to Urban Canopy Models (UCM) are broadly used to interpret and study processes occurring within the Urban Boundary Layer (UBL) such as, the variability of the flow, turbulence fields and thermal impact of cities. These UCM schemes attempt to incorporate the detailed physics of turbulent transport, radiative trapping, and conduction in solid media while keeping the simple geometry of an urban-canyon representation, thus, giving a realistic physical description of the urban areas. Among these processes the Urban Heat Island (UHI) - the existence of higher temperature within cities compared to the surrounding rural areas - has received more attention from the scientific community. The UHI effect occurs due to the altered radiation and energy budget in built-up areas (Landsberg, 1981). Recently, many authors have contributed to a better understanding of the urban areas impact's on the lower atmosphere, showing the ability of the UCMs to reproduce these processes for a large number of different urban and build-up regions (Lo et al., 2007; Lemonsu et al., 2009; Ren et al., 2011).

Salamanca et al. (2011) used the WRF model to study UHI during two consecutive days, when synoptic conditions favoured its formation, and evaluate mitigations strategies for it, over Madrid. Comparing the simulated results to observations the authors have seen that the model was able to reproduce satisfactorily the air temperature. However, wind field over the city is more difficult to validate and is strongly dependent of the mesoscale circulations in the surroundings areas.

In order to evaluate the performance of a urban coupled modelling system Meng et al. (2010) conducted three simulations of a heat wave event which occurred around Guangzhou, using two different land use datasets and a urban canopy model. In their work the authors have concluded that using an UCM the model better reproduces the 2-m temperature evolution, producing the smallest minimum absolute average error. Furthermore, it was shown that most of the incoming energy over urban areas is partitioned into sensible heat flux and, therefore, strongly heating the surface and enhancing the heat wave. On the other hand, during night time, most of the soil heat flux is partitioned into sensible heat flux leading to the development of night time UHI which increases the magnitude and duration of heat waves.

The idealized study of Kusaka and Kimura (2004) demonstrates that single-layer UCMs have a larger volumetric heat capacity and a smaller sky view factor due to the existence of a vertical urban surface, thus changing the energy budget. The authors also showed that when using the UCM the heat island circulation is less intense than when using the atmospheric model with the standard slab urban model. Additionally, the coupling with a UCM delays the phase of surface air temperature, reduces the diurnal range of the temperature, and produces a nocturnal heat island, which results from the difference in atmospheric stability between city and its surroundings.

Not only studies about UHI have been carried but also several authors have shown the importance of urban effects in flow dynamics and energy transport (Rao et al., 2004; Nadeau et al., 2009; Grawe et al., 2012; Wyszogrodzki et al., 2012). Likewise, Lee et al. (2010) studied the performance of different urban surface parametrizations in the WRF model in simulating UBL. These authors performed a set of three simulations over the Houston metropolitan area using a bulk urban parametrization in the Noah land surface model (original LSM), a modified LSM, and a single-layer UCM. The results the authors concluded that the UCM simulation shows the best fit to observed data, reducing the systematic model bias existent in the original LSM simulation and giving a more realistic turbulent energy partitioning. Moreover, sensitivity experiments done by Chin et al. (2005) showed that for a weak urban heat island case, the model horizontal grid resolution is important in simulating the

elevated inversion layer.

In addition, Ohashi and Kida (2002) studied the transport of urban pollution by sea breeze. In their study the authors showed that there is a secondary thermal circulation due to the UHI effect over the urban area that amplifies this transportation.

For a UCM to capture the physics of conductive, radiative and turbulent advective transport of energy it is important to provide it with accurate parameters, including both mesoscale meteorological forcing and microscale surface inputs, given that these fluxes are strongly dependent of the urban parameters that describe the morphology of the city (Wang et al., 2011; Salamanca et al., 2011). However, field measurements of all input parameters used by a UCM are rarely possible. Therefore, the understanding the role of these individual parameters on the sensitivity of model results is essential to determine these parameters uncertainty. The work developed by Wang et al. (2011) shows that model outputs (both critical energy fluxes and surface temperatures) are highly sensitive to uncertainties in urban geometry, whereas variations in emissivities and building interior temperatures are relatively insignificant. Furthermore, sensitivity of the model to input surface parameters is also shown to be very weakly dependent on meteorological parameters. These authors conclude by showing that the UCMs are generally suitable for modelling urban atmosphere energy exchanges, but their performance depends largely on the accuracy of the input parameters. Due to this, in the last few years Ching et al. (2009) have carried out an effort to provide detailed urban canopy parameters to improve the parametrisations of UBL processes in the USA region.

The UHI effect in Lisbon city it is well known and has been broadly studied by Alcoforado et al. (2009) and Alcoforado and Andrade (2006), using measurements and geospatial classification. However, few studies using numerical models coupled with UCMs can be found for this region. Given this, this work aims to evaluate the sensitivity of two UCMs existent in the WRF model, to study the influence of these models on the atmospheric proprieties within the UBL and the atmospheric layers above it.

Chapter 6

Method and Data

The UCMs adopted by the WRF model have been extensively tested against field measurements giving satisfactory results (Lee et al., 2010; Salamanca et al., 2011; Wang et al., 2011). Furthermore, it has been seen that this modelling approach is computationally efficient as compared with computational fluid dynamics models that resolve all the processes involved in the urban canopy (Wang et al., 2011; Wyszogrodzki et al., 2012). Given so, in this work the WRF-ARW version 3.4 was used (Skamarock et al., 2008) for the analysis of model results response to the choice of the UCM parametrisations applied along with the inclusion to new data sets of topography and land use. Initial and lateral boundary conditions from GFS analyses (NCEP, 2003) were provided to the model at a three hour interval as well as high resolution sea surface temperature data on hourly bases (Gemmill et al., 2007). The default WRF lower boundary conditions showed differences when compared to the high resolution data sets, as one can see for land use - Figure 6.1. Thereupon, the SRTM and CORINE datasets were used for topography and land use, respectively (Description of the data at the Introduction chapter).

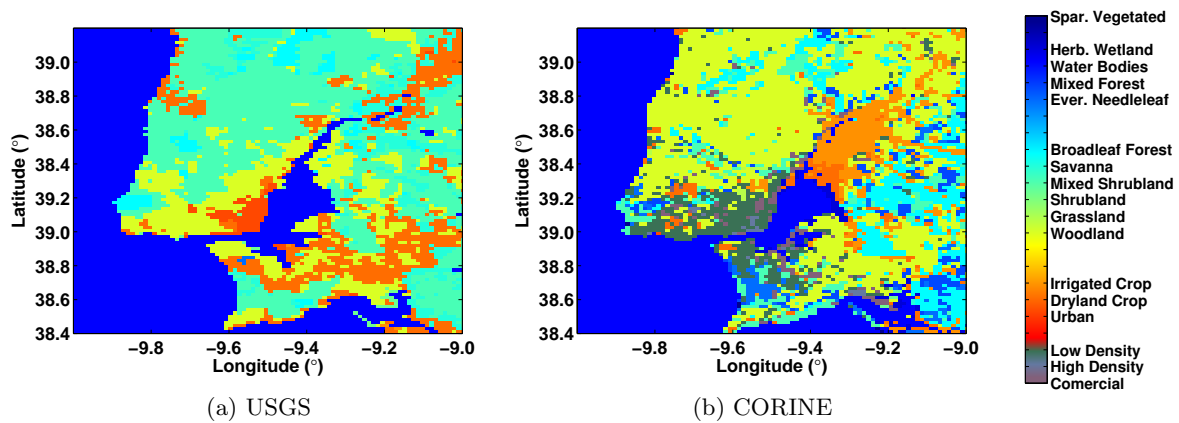


Figure 6.1: Land use categories for the default WRF configuration (USGS) and for the CORINE land use dataset



Figure 6.2: Study area map showing the Lisbon region location in the Iberian Peninsula, Maps from googlemaps.com.

The study area is centred over Lisbon region - Figure 6.2 - in the western Portuguese shore. Lisbon

is the Portuguese capital and larger Portuguese city, being situated in the mouth of Tagus river.

Given the main objective of this work, a period in which atmospheric conditions favour the development of large UHI over the Lisbon region was considered. The period in which these conditions are met was found in July 29th of 2010. During this day the Iberian Peninsula was under the influence of an high pressure pattern centred near Azores archipelago - Figure 6.3. Subsequently, the strong surface heat due to this synoptic setting lead to the development of a thermal low over the Iberian Peninsula.

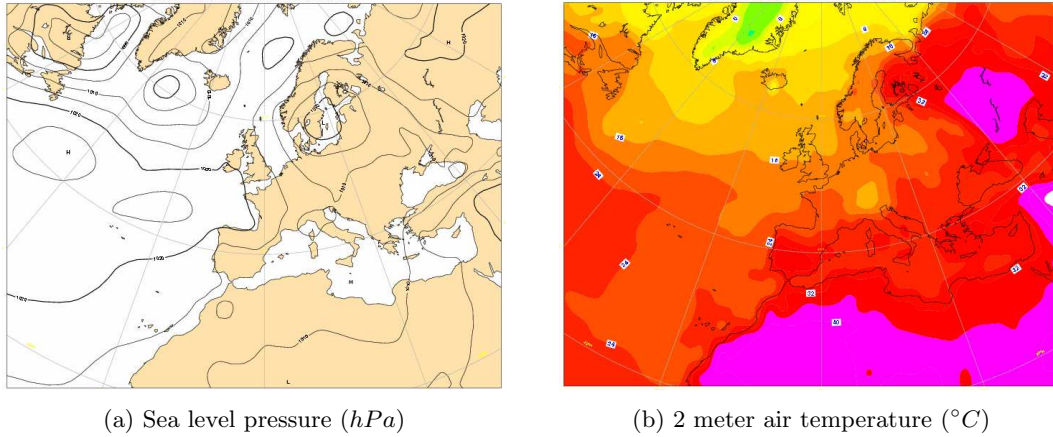


Figure 6.3: Synoptic situation for July 29th at 12:00 UTC (ERA Interim, daily fields)

Thereupon, the considered period under analysis starts in July 29th, 2010 and is extended to the following five days during which these conditions persisted.

Three two-way nested domains using grid nudging to the GFS analysis was applied to the study area - Figure 6.4. In the nested domains one can find a parent domain (d01) with an horizontal resolution of 25 km, and two nested domains (d02 and d03) with an horizontal resolution of 5 and 1 km, respectively.

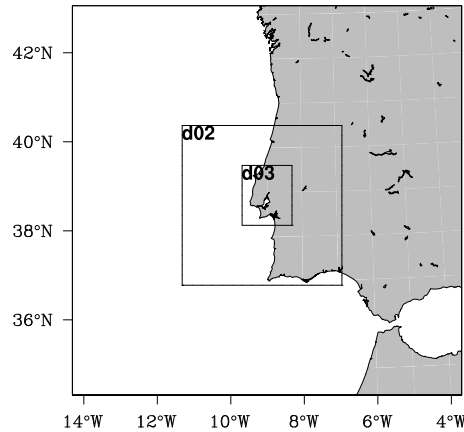


Figure 6.4: Three nested model domains used in WRF.

When trying to use the model configuration proposed by Ferreira (2007), high vertical velocities arise near the surface making the model numerically unstable. These numerical instabilities crashed the model after a few hours of simulation, producing results with no physical significance. In order to achieve numerical stability, several configurations were tested and a set of filters were applied. Namely, a 1-2-1 filter with three passes was applied to the topography field of domain 3 as for the parent domain data. Also, in order to prevent the model from becoming unstable with locally large vertical velocities, vertical velocity damping was applied as suggested by Skamarock et al. (2008). In addition, positive definite 6th Order Horizontal Diffusion was used.

The set of parametrisations used in model configuration were the WRF Single-Moment 6-class

scheme microphysics (Hong and Lim, 2006), Dudhia shortwave radiation scheme (Dudhia, 1989), Rapid Radiative Transfer Model (RRTM), longwave radiation model (Mlawer et al., 1997), the Eta similarity surface layer scheme (Skamarock et al., 2008), the Noah Land Surface Model (Chen and Dudhia, 2001) and Bougeault and Lacarrere PBL scheme (BouLac) (Bougeault and Lacarrere, 1989). In terms of cumulus parametrization, the Kain-Fritsch scheme was used (Kain, 1993). These sets of parametrisations were also used by Wyszogrodzki et al. (2012) in their work with the coupled system WRF/UCM giving satisfactory results.

The WRF model presents two different UCMs, namely the Single Layer Urban Canopy (SLUCM) (Kusaka et al., 2001) and the Multi-layer Urban Canopy Building Effect Parameterization (BEP) (Martilli et al., 2002). A resumed description of the WRF UCMs are shown in Table 6.1 and the information introduced in the PBL scheme in Table 6.2

Table 6.1: Description of the WRF UCMs features - Table adapted from Wyszogrodzki et al. (2012).

SLUCM	BEP
<ul style="list-style-type: none"> - Urban geometry is represented through orientation of the infinitely long street canyons, and three different surface types: roof, wall, and roads. - Diurnal change of solar azimuth angle. - The multi-layer heat equation for the roof, wall and road interior temperatures. - Anthropogenic heat. - Effects of shadowing from buildings, trapping and reflection of radiation. - An exponential wind profile in the canopy layer. - Thin bucket model for hydrological processes. 	<ul style="list-style-type: none"> - Three-dimensional box type urban surfaces. - Percentage of urban area is defined. - Buildings vertically distribute sources and sinks of heat and momentum through the whole canopy layer. - Effects of the walls, streets and roof surfaces on momentum, turbulent kinetic energy, and potential temperature. - Shadowing, reflection, and trapping of shortwave and longwave radiation in the urban canyons.

Table 6.2: Description of the WRF UCMs information introduced in the PBL scheme - Table adapted from Wyszogrodzki et al. (2012).

SLUCM	BEP
<ul style="list-style-type: none"> - Surface skin temperature and heat fluxes of the roof, wall and roads. - Energy and momentum exchange coefficients for urban surface. 	<ul style="list-style-type: none"> - Modification of the length scales induced by the presence of the buildings. - Weighted averaged source/sink coefficients and length scales accounting for the percentage of urban and vegetated areas.

As described in Section 3 of Part I, a recategorization was performed to the CORINE data set to be recognizable by the WRF model as described by Pineda et al. (2004). For the UCMs sensitivity tests, the eleven CORINE urban classes were converted into high density residential, low density residential and commercial/industrial/transportation, as described in Table 6.3.

The parameters used in the three different urban classes for each UCM to characterize the Lisbon urban area geometry are described in Table 6.4.

To conduct the sensitivity study, a simulation using the BEP UCM (BEP) and a simulation using SLUCM UCM (SLUCM) have been performed. Due to the vertical levels permitted by the UCMs options a different number of vertical levels was used in these simulations, namely, 34 for BEP and 33 for SLUCM simulation. In order to have vertical compatible comparison two control simulations with no use of UCM were configured. The control simulation for BEP with 34 vertical levels (CTL34) and the control simulation for SLUCM with 33 vertical levels (CTL33). These vertical levels differ only in the first level, thus, in the 34 levels simulations the top of the vertical level closest to the surface is located at an height of ~ 20 m. In the 33 levels simulations this level is removed, and the top of the first level above ground is located, at an height of ~ 50 m.

The UCMs are only activated for the higher resolution domain - d03 - forthwith, all the analysis

Table 6.3: Recategorization process used to convert the eleven urban CORINE into the three USGS urban classes used by WRF UCMs.

CORINE ID	Description	USGS ID	Description
111	Continuous urban fabric	32	High Density Residential
112	Discontinuous urban fabric		
141	Green urban areas	31	Low Density Residential
142	Sport and leisure facilities		
121	Industrial or commercial units		
122	Road and rail networks		
123	Port areas		
124	Airports	33	Commercial/Ind./Transp.
131	Mineral extraction sites		
132	Dump sites		
133	Construction sites		

Table 6.4: Resume of the principal parameters used to describe Lisbon metropolitan area geometry in the WRF/UCM model.

Parameter	Class ID	SLUCM	BEP
	High Density Residential	15	10 20 % 15 60 % 20 20 %
Roof Level (<i>m</i>)	Low Density Residential	10	5 15 % 10 70 % 15 15 %
	Commercial/Ind./Transp.	24	15 10 % 20 25 % 25 40 % 30 25 %
Roof Width (<i>m</i>)	High Density Residential		9.4
	Low Density Residential		8.3
	Commercial/Ind./Transp.		10
Road Width (<i>m</i>)	High Density Residential		9.4
	Low Density Residential		8.3
	Commercial/Ind./Transp.		10
Green Fraction (%)	High Density Residential		10
	Low Density Residential		50
	Commercial/Ind./Transp.		5

will be focused in this domain.

Initially, the characterization of the atmospheric conditions for the period under study will be made for the control experiments. Focusing on the assessment of the WRF model sensitivity to UCM choice, the difference fields related to temperature, wind flow and energy budget between the UCM experiments and the respective control simulations will be analysed. Furthermore, as several authors have shown, changes in energy budget and turbulent fields can be changed when using WRF surface parametrizations coupled with UCM, hence, the difference fields for turbulent kinetic energy (TKE) will also be analysed. Finally, a more detailed study of simulated hourly temperature and wind was done by comparison with observed hourly data. A skill analysis for every experiment was performed, making possible to evaluate the performance of the UCMs simulating this particular case study.

With the intent to isolate the turbulent variations from the large-scale ones, the partition of the variables into mean and turbulent components was made. Given a certain variable (Q):

$$Q = \overline{Q} + Q' \quad (6.1)$$

where \overline{Q} was considered to be the 30 minute average using two minute interval data and Q' is the perturbation around the basic state.

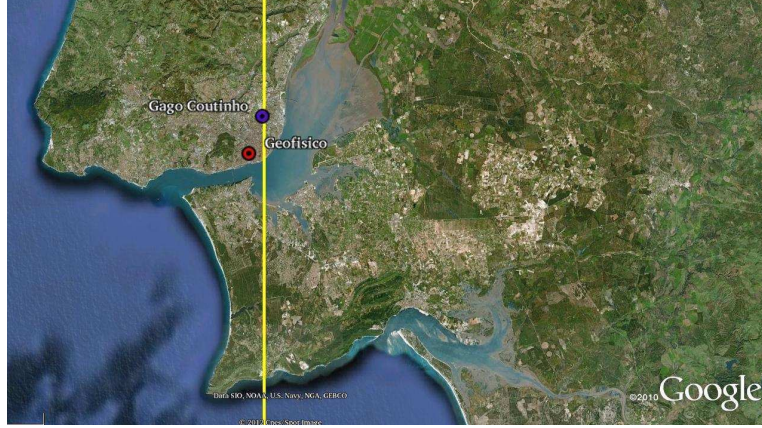


Figure 6.5: Location of the weather stations over Lisbon Region (blue and red dot and the location of the cross section used in this work (yellow line)).

Table 6.5: Weather Stations information used to evaluate model skill.

Location	Latitude ($^{\circ}$)	Longitude ($^{\circ}$)	Altitude (m)
Geofisico	38.72	-9.14	77
Gago Coutinho	38.76	-9.13	104

Two weather stations were considered - Geofisico and Gago Coutinho - These stations are owned and operated by the Portuguese Meteorological Institute and both present temperature (at a 2 *m* high) and wind data (at a 10 *m* high) for the simulated period. In addition, Gago Coutinho station has daily radiosonde data for temperature, wind speed and direction. The location of these stations can be seen in Figure 6.5. Details on these stations can be found in Table 6.5.

To produce vertical profiles of the atmospheric properties, a meridional cross section was considered at a longitude of $9.1268^{\circ} W$, for all latitudes within the higher resolution domain - d03 - as can be seen in Figure 6.5.

In order to analyse the model performance for all simulations and compare them, the same error measures described in Chapter 3, as well as the skill criteria were applied.

Chapter 7

Results and Discussion

7.1 Atmospheric Situation

As described in the previous Chapter the synoptic situation for the period under analysis favours strong atmospheric heating over the Lisbon region.

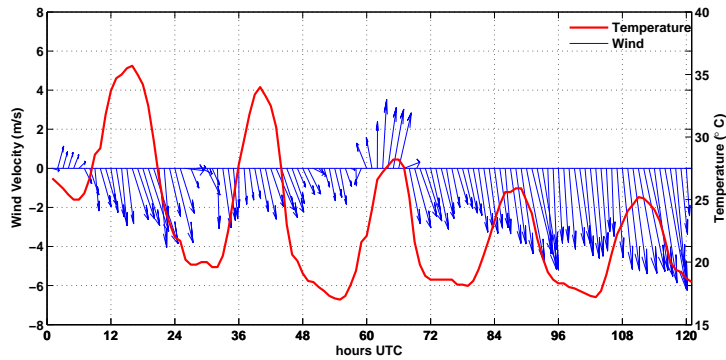


Figure 7.1: Time series for two meters high air temperature ($^{\circ}C$) in red and wind intensity ($m \cdot s^{-1}$) in blue for Gago Coutinho station.

Figure 7.1 shows the time series of 2-m air temperature ($^{\circ}C$) in red and 10-m wind intensity ($m \cdot s^{-1}$) in blue for Gago Coutinho station. It is evident that the period under analysis can be divided into two sub-periods, a first one in which temperature is high, reaching a maximum temperature of $\sim 35^{\circ}C$ - in the first two days - and a period in which the maximum temperature does not exceed the $27^{\circ}C$ - the three following days. These sub-periods can also be identified in the observed wind data. In the figure, one can see that the first sub-period is characterized by a synoptic low intensity wind regime, intensifying along the day and weakening during night time, accompanying the sea-land breeze circulation development, and weakening during night time. This low intensity wind regime may favour the atmospheric heating within Lisbon City as low advection tends to keep warm air within the city. Later, in the second sub-period a stronger wind settles in which makes the sea breeze development not evident in the observed wind data. This fact may indicate that a strong synoptic scale wind becomes dominant. This high intensity flow may favour the ventilation of Lisbon City and consequently its cooling. However, it is noticeable that for the third day of simulation - between the 60 to 72 hours in Figure 7.1 - wind flows from south due to a weakening of synoptic circulation and therefore regional processes become prevalent.

Given this, due to the distinct characteristics in the period under study, the analysis presented here may also focus on these sub-periods separately. The third day of simulation was excluded in order to get consistency of weather patterns in these sub-periods.

During the simulated period the atmosphere presents stratified stability - Brunt-Väisälä frequency greater than $\sim 0.01s^{-1}$. In a thin layer above the first kilometre from the surface a very stable layer develops with a Brunt-Väisälä frequency greater than $0.035 s^{-1}$). However, just near the surface, due to the strong surface heating that occurred in this period, an unstable layer develops. Furthermore, a gap of highly stable environment forms close to the surface at $38.7^{\circ}N$, due to the presence of the Tagus river. Albeit presenting distinct features of temperature and wind data for the period under analysis, atmospheric stability presents the same behaviour throughout all the sub-periods.

The characteristics found in the atmospheric conditions over Lisbon metropolitan area - high surface heating, instabilities near the surface and high stability above the first kilometre - favours the

generation of gravity waves.

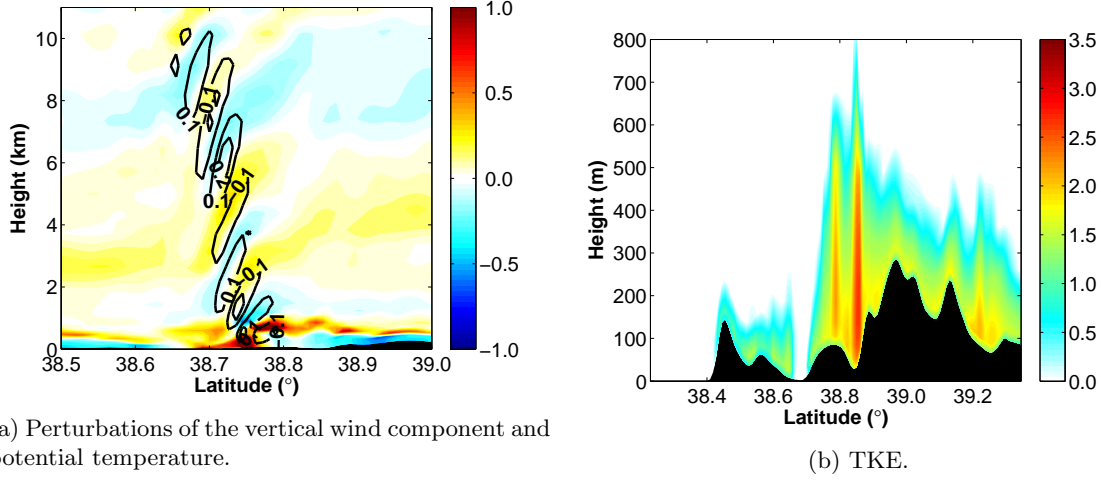


Figure 7.2: Vertical cross section for the perturbations of the vertical wind component (shaded $m \cdot s^{-1}$) and potential temperature ($^{\circ} C$) contours (7.2a) and Turbulence Kinetic Energy ($m^2 \cdot s^{-2}$) (7.2b) in July 29th at 13:00 UTC CTL34 simulation.

Figure 7.2a represents the perturbations for the vertical wind component in shaded ($m \cdot s^{-1}$) and for potential temperature ($^{\circ} C$) contours in July 29th at 13:00 UTC for CTL34 simulation. A wave like behaviour for both perturbations. Furthermore, it can be seen that the vertical wind component perturbation is in quadrature with the potential temperature perturbation, pattern that its known to be a characteristic of gravity waves (Holton, 2004). Thereupon, one may conclude that in this day there is strong gravity wave activity over this area.

Nonetheless, one can see that these gravity waves are generated in this location over the Lisbon region coincident with the location of the frontier between land and Tagus river. As seen before, in this area there is the development of a very high stability zone, thus, the presence of the gravity waves in this single location may indicate that they might be generated by the interaction of the wind flow - flowing from North - the surface high temperatures and the barrier created by the stability over Tagus river. The intense development of gravity waves over this region combined with the high stability may be the reason for the difficulties found when trying to run the model with the default configuration.

Due to the fact that the first sub-period under study is the one with the optimal conditions for gravity waves development, these marked characteristics can only be seen in this sub-period. In the second sub-period, the high wind intensity and weaker surface heating makes the atmosphere not suitable for the development of these waves.

Figure 7.2b shows the Turbulence Kinetic Energy (TKE) ($m^2 \cdot s^{-2}$) for July 29th at 13:00 UTC in CTL34 simulation. TKE quantifies the intensity of turbulence and it is directly related to momentum, heat and moisture transport throughout the boundary layer. One can see that large values for TKE are only observed in the first hundred of meters near the surface. Also, a gap with no TKE can be seen over Tagus river and the ocean - south of 38.4° N - due to the high stability present in both these areas. Furthermore, near the location where gravity waves are generated one can see that high values of TKE are present, which indicate that gravity waves may be generated in this area due to turbulence caused by the interaction of wind flow, surface temperature and stability, perturbing the highly stable levels of the atmosphere above the surface.

The TKE budget equation can be described as (Stull, 1988):

$$\frac{\partial \bar{e}}{\partial t} + \bar{u}_j \frac{\partial \bar{e}}{\partial x_j} = \delta_{i3} \frac{g}{\theta_v} \left(\overline{u'_i \theta'_v} \right) - \overline{u'_i u'_j} \frac{\partial \bar{u}_i}{\partial x_j} - \frac{\partial \left(\overline{u'_j e} \right)}{\partial x_j} - \frac{1}{\bar{\rho}} \frac{\partial \left(\overline{u'_i p'} \right)}{\partial x_i} - \epsilon \quad (7.1)$$

where e represents the TKE, u the wind velocity, g the gravity, θ_v the virtual potential temperature, ρ the air density, p the pressure and ϵ the term that represents the viscous dissipation of TKE. The overbar indicates the time average.

The fourth term of the second member in Equation 7.1 is a pressure correlation term - Equation 7.2 - that describes how TKE is redistributed by pressure perturbations. This term is often associated with oscillations in the air - gravity waves - (Stull, 1988). Stull (1988) shows that turbulence within a stable boundary layer can be lost in the form of waves. Hence the pressure correlation term acts not only to redistribute TKE in the boundary layer, but can also radiate energy from the boundary layer.

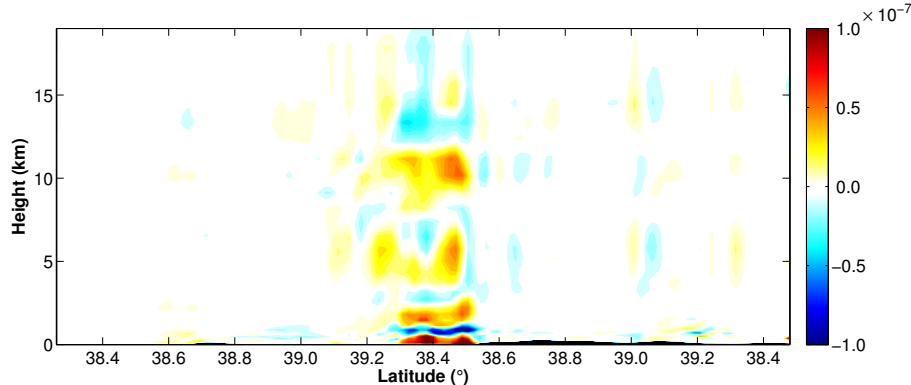


Figure 7.3: Vertical cross section for the pressure correlation term ($m^2 \cdot s^{-2}$) for July 29th at 13:00 UTC CTL34 simulation.

$$-\frac{1}{\bar{\rho}} \frac{\partial (\overline{u_i' p'})}{\partial x_i} \quad (7.2)$$

Given this, the analysis of this term magnitude's gives important information of the interaction of the gravity waves with the atmosphere. Figure 7.3 shows the cross section for the pressure correlation term ($m^2 \cdot s^{-2}$) for July 29th at 13:00 UTC CTL34 simulation. As can be seen in this figure, near the surface, where turbulence is intense, the pressure correlation term contributes to magnify the TKE budget. Immediately above the surface one can see a zone where the TKE decreases, this zone correspond to an highly stable layer, which may indicated that in this area gravity waves will use TKE. The development of gravity waves in this region interacts with the TKE budget using this energy to propagate through the upper levels.

7.2 Sensitivity to the UCMs

As seen before, when using an UCM coupled with the WRF model a different variety of processes concerning buildings are modelled through parametrisations introducing changes in the energy budget and flow patterns. Thus, when using an UCM changes are expected near the surface for temperature, wind flow or even TKE.

The difference of the urban land use categories between the control and UCM simulations for CORINE dataset can be seen in Figure 7.4. The most common urban category in the region is the low density residential, high density residential grid cells are found mostly in the centre of Lisbon City and commercial/industrial zones are found in the periphery.

In Figure 7.5, the difference for 2-m mean air temperature ($^{\circ} C$) between SLUCM 7.5b BEP 7.5c and their respective control simulation for the first sub-period - July 29th and 30th is shown as well as the 2-m mean air temperature for CTL34 Simulation. Here, one can see that, for this sub-period, using an UCM there is a decrease of temperature of approximately $0.5^{\circ} C$ in Lisbon surroundings and a decrease of about $1.0^{\circ} C$ in Lisbon City region. Furthermore, it can be seen that this cooling effect is more pronounced for SLUCM simulation, where model results show that for this sub-period this difference can reach $-1.5^{\circ} C$ when comparing with the control simulation. Furthermore, for the first sub-period, the difference of air temperature is more pronounced at night time than for day time, when differences between UCM simulations and their control can be as large as $2^{\circ} C$.

Albeit not shown here, for the second sub-period under analysis a similar pattern was observed for 2-m air temperature mean difference. However, for this sub-period differences are smaller for both

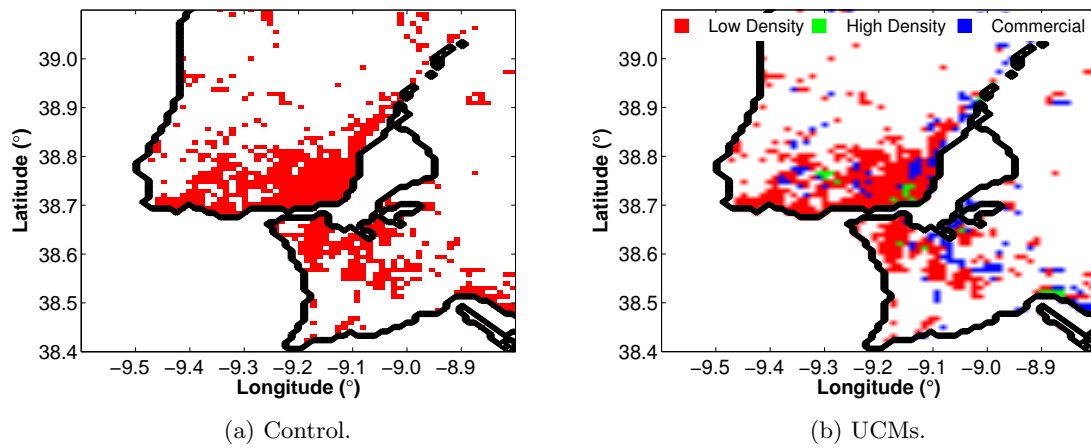


Figure 7.4: Urban land use category location, on (a) control simulations and (b) UCMs simulations.

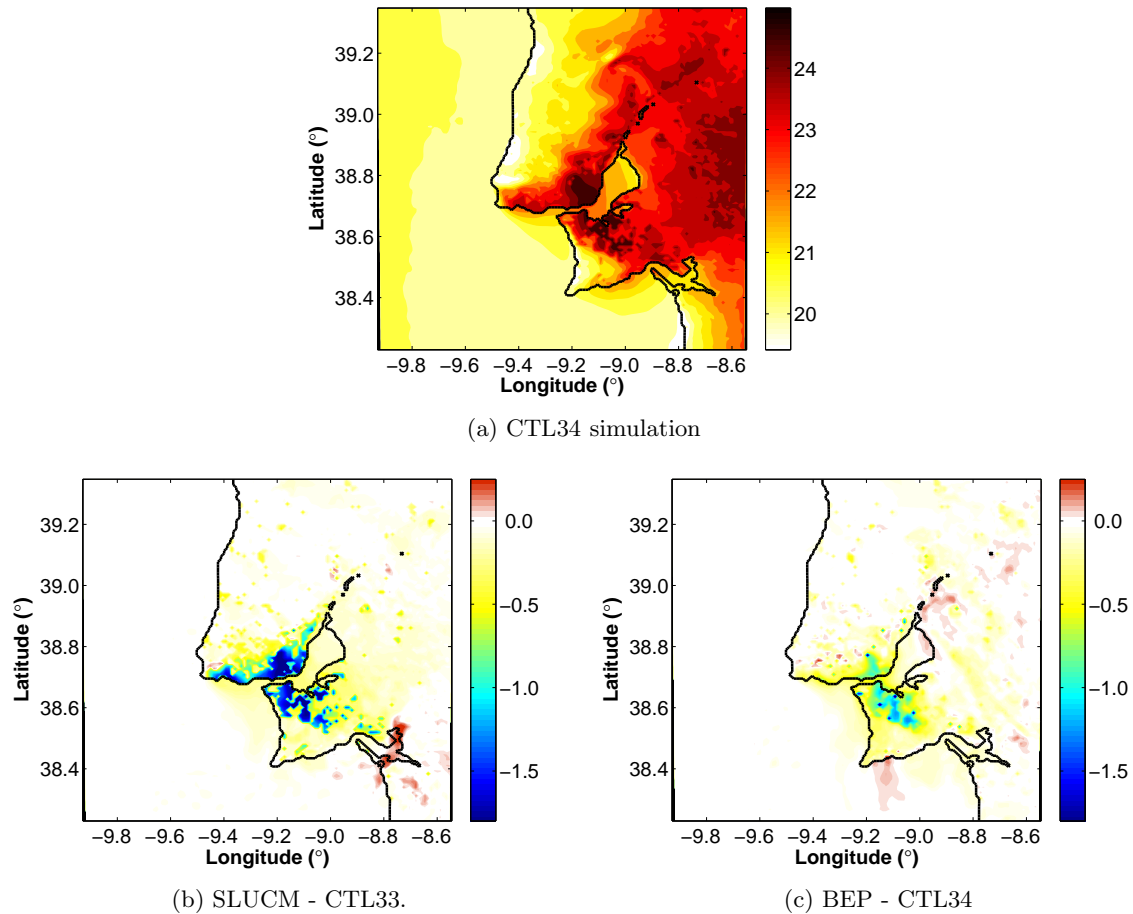
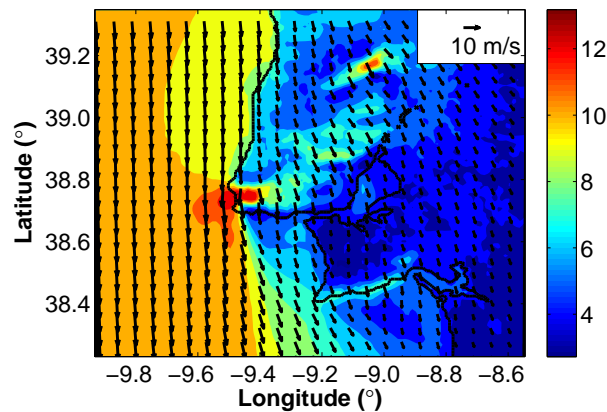


Figure 7.5: 2-m mean air temperature ($^{\circ}C$) for (a) CTL34 Simulation, (b) difference between SLUCM and CTL33 simulations and (c) difference between BEP and CTL34 simulation during the first sub-period - July 29th and 30th.

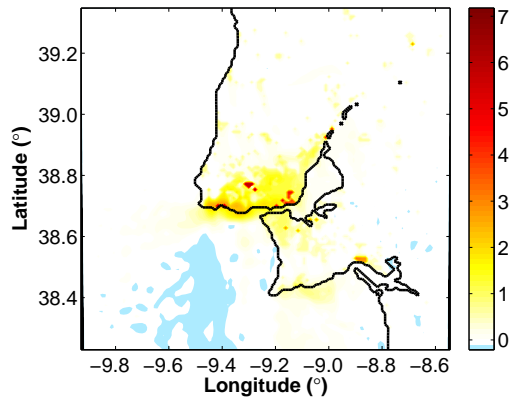
simulations ($< 0.5^{\circ}C$) and the minimum values are located in the southern margin of the Tagus river, as shown in Figure 7.5. Contrary to the first sub-period, here differences in temperature are homogeneous during the time span.

Given the model configuration described earlier (Table 6.4), one can see that this cooling effect may be associated with the green area fraction considered for each urban class - 50 % green fraction for low density residential. In the control simulations land surface processes are parametrised by the Noah Land Surface Model (Noah LSM) that considers a 10 % of green fraction in urban areas. Since, vegetation enhances cooling by evapotranspiration, this leads to a decrease of temperature in the UCM simulations where the green fraction is higher for the most represented urban class.

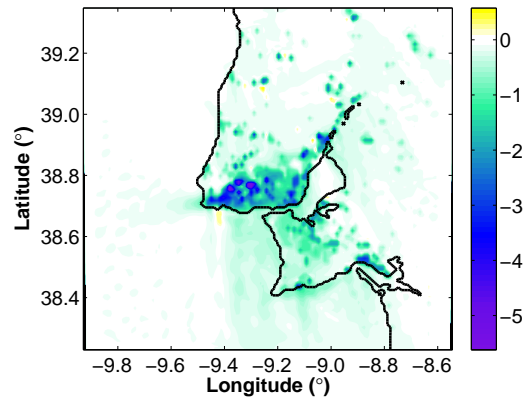
Besides the difference in green fraction between the UCMs and the Noah LSM, other differences must be taken into account. Likewise, Noah LSM considers an albedo of 15 % and both UCMs a value 20 % which can result in a warming in the control run. However, these processes are quite complex and their influence can differ in the atmospheric conditions present at the time. As mentioned before, the Noah LSM represents the urban areas as a flat surface with a roughness length of 1 *m* whereas the UCMs compute the effects of the city geometry as drag and exchange of momentum.



(a) 10 *m* mean wind speed (shaded) and direction (arrows)
CTL34 simulation



(b) SLUCM - CTL33.



(c) BEP - CTL34

Figure 7.6: 10-m mean wind speed and direction ($m \cdot s^{-1}$) for (a) CTL34 Simulation, b the difference between SLUCM simulations and c the difference between BEP simulation during the second sub-period - August 1st and 2nd.

Figure 7.6 shows the difference for 10-m mean wind speed ($m \cdot s^{-1}$) between SLUCM (Figure 7.6b) BEP (Figure 7.6c) and their respective control simulation for the second sub-period - August 1st and 2nd. Additionally, Figure 7.6a shows the 10-m mean wind speed and direction for the CTL34 Simulation. It can be seen that in the SLUCM simulation most differences in the domain introduced by the UCM are positive, showing an increase of wind speed over the urban area when compared to its control simulation. On the other hand, the BEP simulation shows a decrease of wind speed over

the urban area. The same differences pattern can be observed for the first sub-period (not shown). However, those differences are smaller due to the weaker wind flow intensity that characterize this sub-period.

This opposite result for the two UCMs - SLUCM and BEP - mean that albeit using the same urban geometry, the different methods and processes solved by the UCMs have a significant impact in flow characteristics over the urban area. BEP solves more complex physics than the SLUCM. BEP uses multi-layers in the atmospheric boundary layer and computes the effects of the walls, streets and roof surfaces on momentum and turbulent kinetic energy resulting in higher drag over the urban area.

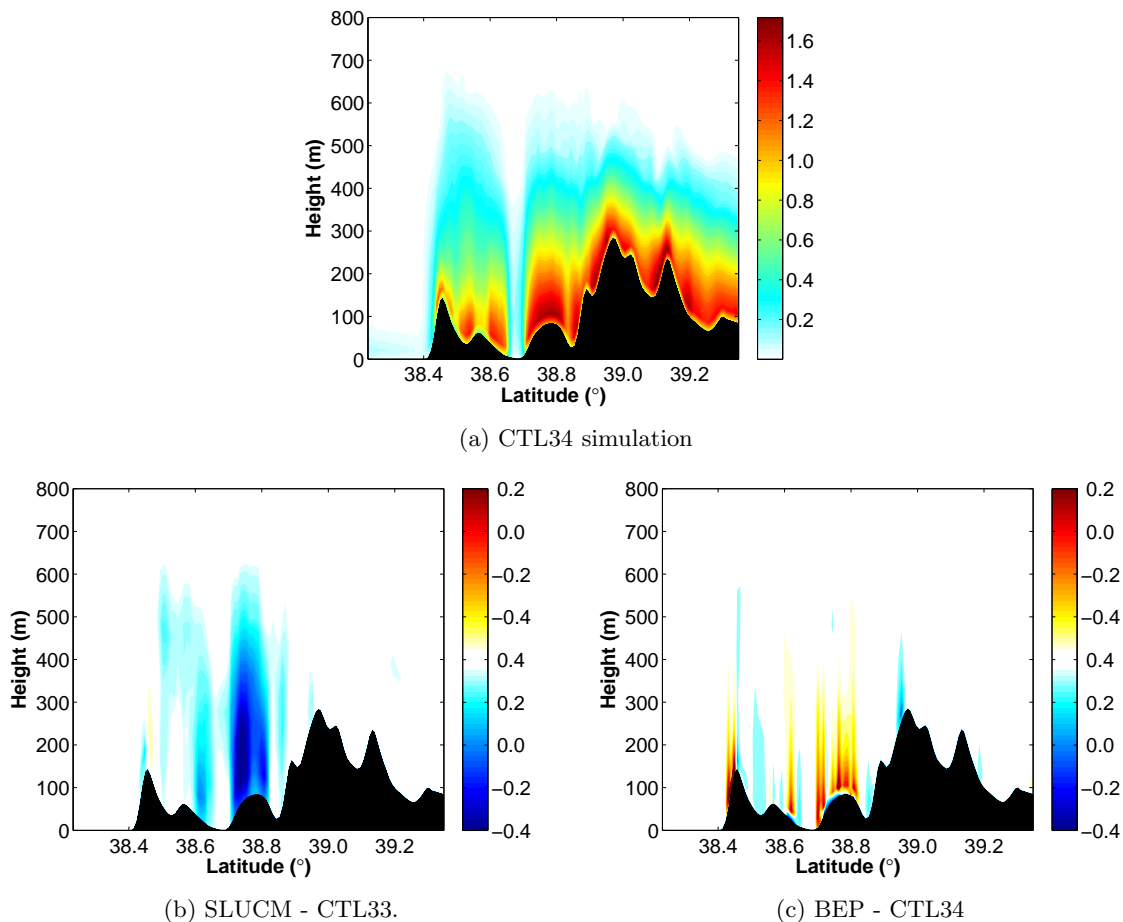


Figure 7.7: Cross section (South-North) for the day time mean TKE ($m \cdot s^{-2}$) for (a) CTL34 simulation, (b) the difference between SLUCM simulation and (c) the difference between BEP simulation for all simulated period.

As mentioned earlier, the PBL is the part of the troposphere that is directly influenced by the presence of earth's surface. Given this, it is expected that the use of different methods to solve processes within the UC can change turbulent processes in the lower levels of the atmosphere, which consequently can result in different values for the PBL height .

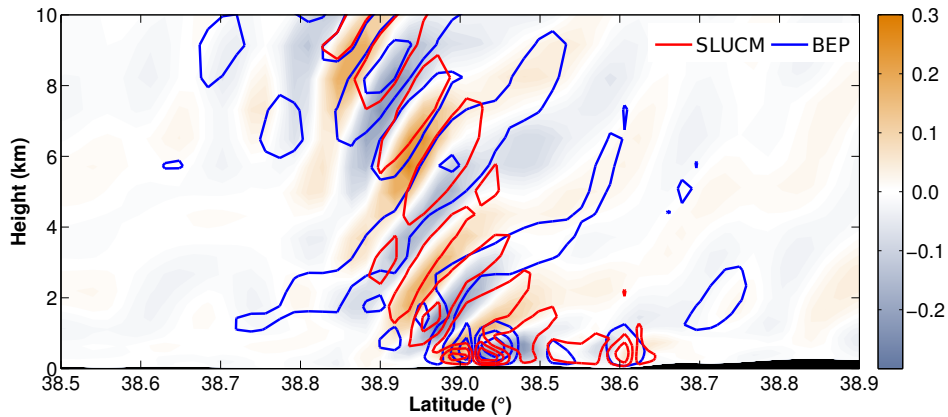
Model results show that during day time - when turbulent processes are dominant - there is a clear tendency for BEP to present higher values of PBL height than CTL34 - $\sim 150 m$ higher - suggesting that the wind flow weakening that was found, when compared with the control simulations, is converted into turbulence by the exchange of momentum from the surface to the atmosphere. On the other hand, SLUCM presents lower values than its control simulation - $\sim 150 m$ higher.

Nonetheless, at night time, when turbulent processes are not dominant, atmospheric stability is higher and turbulent processes occurring within the UC are less intense and the UCMs have the same behaviour as their control simulations.

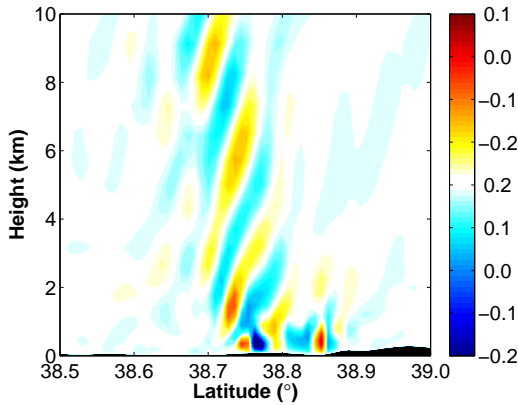
These differences found for PBL height shows that the use of UCMs has a significant impact

in solving the turbulent processes occurring within the PBL in urban areas, especially at day time. Moreover, different UCMs can have distinctive results for a similar urban geometry with significant differences associated to TKE budget.

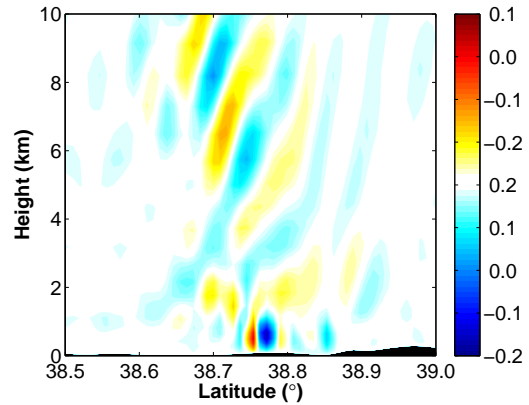
Figure 7.7 shows the day time mean TKE for CTL simulation - 7.7a - and the day time mean TKE difference between SLUCM and BEP and their control simulations - 7.7b and 7.7c respectively. It can be observed that SLUCM produces less TKE over the urban area than BEP simulation. However, differences propagate higher in SLUCM than in BEP. It can also be observed that differences in TKE over the urban area seen in BEP simulation are more localised than those found in SLUCM. The changes introduced in TKE near the surface, in combination with the atmospheric conditions present in the simulated period, it is expected that the use of an UCM may affect the forcing of gravity waves generation, previously observed in Figure 7.2 according to the more/less availability of TKE to feed these perturbations.



(a) Vertical wind component perturbations



(b) SLUCM - CTL33.



(c) BEP - CTL34

Figure 7.8: Cross section (South-North) for (a) the vertical wind component perturbation ($m \cdot s^{-1}$) (shaded) for CTL34 simulation and difference between SLUCM (red line) and between BEP (blue line), (b) the difference between SLUCM and CTL33 simulations and (c) the difference between BEP and CTL34 simulations, for July 29th at 13:00 UTC.

Figure 7.8 shows a cross section for the vertical wind component perturbation for CTL34 and the difference of vertical wind component perturbations between SLUCM and BEP, and their respective control simulations (Figure 7.8a) for July 29th at 13:00 UTC. In addition, the cross section for the difference for vertical wind component perturbations between SLUCM and CTL33 simulation (Figure 7.8b) and BEP and CTL34 simulation (Figure 7.8c) is also shown for the same instant. One can observe that the differences introduced by the UCMs in the lower levels propagate through the whole troposphere and interact with the generated gravity waves. Moreover, it can be seen that for both UCM simulations there is a change in perturbations amplitude near the surface. Over Lisbon City

the UCM perturbation intensifies - positive difference - whereas in the northern vicinity of the city a negative difference for perturbation can be observed in SLUCM and BEP simulations. In addition, looking to Figure 7.8a one can see that the use of an UCM introduces a spatial lag in gravity waves amplitude phase. Furthermore, there is an amplification of gravity waves amplitude when an UCM is used. However, the differences of the perturbation at surface are being similar for both SLUCM and BEP. Despite the lower TKE available in SLUCM simulation, this simulation shows an amplification of gravity waves amplitude throughout the whole extent of the troposphere. On the other hand, BEP shows a smaller amplification in the mid troposphere - two to six kilometres - and greater amplification in the upper levels. Nonetheless, for BEP a widening of the gravity waves can also be observe. One can see that the differences caused by the use of the coupled UCMs not only affects the atmosphere near the surface - PBL - but also can create perturbations that can propagate throughout the upper levels and interact with pre-existing gravity waves.

Given this, changes found for the pressure correlation term of the TKE budget may help understand the interaction between the UCMs and the pre-existing gravity waves.

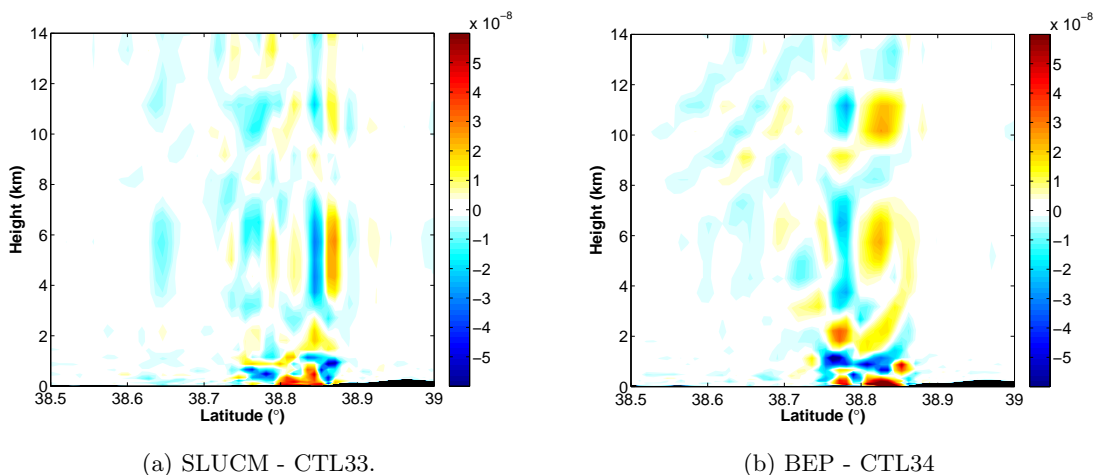


Figure 7.9: Cross section (South-North) for the pressure correlation term of the TKE budget equation difference ($m^2 \cdot s^{-2}$), (a) between SLUCM and CTL33 simulation and (b) between BEP and CTL34 simulation, July 29th at 13:00 UTC.

Figure 7.9 shows a cross section for the pressure correlation term of the TKE budget equation difference between SLUCM and CTL33 simulations 7.9a and BEP and CTL34 simulations 7.9b, in July 29th at 13:00 UTC. There is a change of the TKE budget due to fluctuations in pressure. Namely, near the surface, there is an increase - positive difference - of this term, therefore one may conclude that there is more TKE being generated in this area when using the UCM. Just above the surface, where a layer with high stability is located, there is more TKE being consumed by the pressure perturbations for BEP simulation. This result may be related to the weakening of gravity waves as mentioned before for this simulation. On the other hand, for the same region, SLUCM presents a thin layer with an increase of TKE budget which is probably associated to the increase of gravity wave amplitude in this area.

For the upper troposphere, both simulations present a scattered behaviour of the pressure correlation term differences. This behaviour may result from changes found in gravity waves location and dispersion which may result in a redistribution of the TKE due to pressure perturbations.

7.3 Modelled results vs Observed data

Earlier, a comparison between the UCMs and their respective control simulations showed differences in surface parameters such as temperature and energy budget. It was also shown that these changes affected the upper levels by interacting with gravity waves. In order to understand which simulation represents best the available observations during the simulated period, the comparison of modelled results with observation data was performed.

In this section the comparison of all simulations against observed data at the two surface stations was performed, using Taylor diagrams and combined errors chart. Furthermore, results were also compared to radiosonde data recorded every day at Gago Coutinho station.

7.3.1 Surface Observations

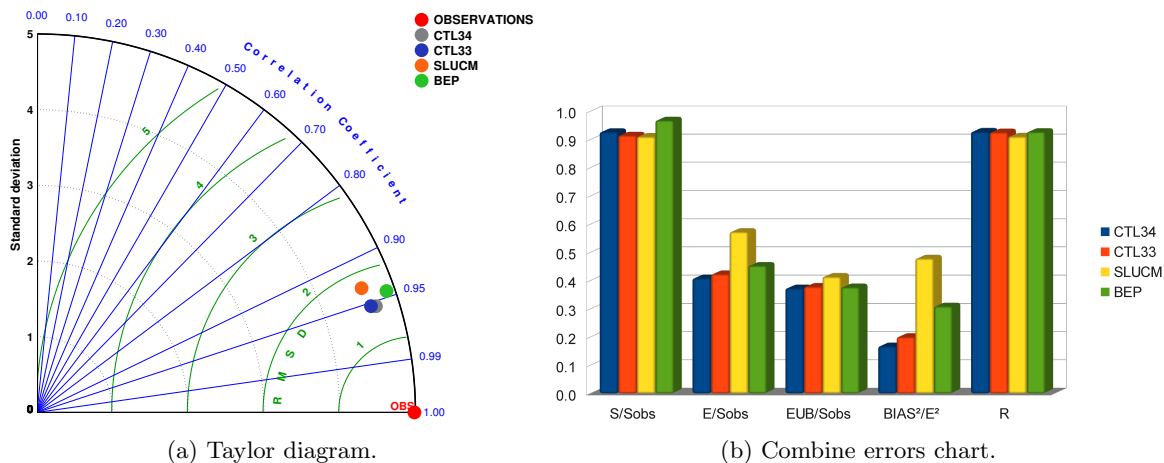


Figure 7.10: Taylor diagram and combined errors chart for temperature for all the simulated period.

The Taylor diagram and the combined error chart for the 2-m temperature for the simulated period are shown in Figure 7.10. One can see that all simulations present high skill simulating near surface temperature, according to all defined skill criteria - Figure 7.10b. However, some differences can be observed between simulations. For instance, both UCM simulations present higher RMSE and weak correlations when compared to the observations. However, BEP represents better the variability found in the observed data. Skill measures present the same characteristics for the two sub-periods under analysis (not shown). For both sub-periods UCM simulations present slighter higher RMSE than their control. However the variability is better represented in the second sub-period by the control simulation and SLUCM than by BEP simulation.

Given this, one can see that the control simulations have a better skill when simulating this atmospheric property but, the differences found between simulations are small.

In Figure 7.11, the Taylor diagram - 7.11a and 7.11b - and the combined error chart - 7.11c and 7.11d - for both u and v wind components for all the simulated period are shown. Here, it is possible to observe considerable spread between the UCM simulations and the observed data. Despite the lower RMSE when compared with all the other simulations, BEP presents greater standard deviation of the error, misrepresenting the observed variability. In addition, it can be seen that SLUCM presents higher error than all other simulation and overestimates the observed variability for u and v wind components. Furthermore, it can be seen that SLUCM overestimates the wind speed, as can be observed by the large amplitude errors - Figures 7.11a and 7.11b. On the other hand, both control simulations - CTL34 and CTL33 - have a high skill simulating both wind components, as can be seen in Figures 7.11a and 7.11b.

Similarly to what has been found for temperature, the characteristics of the error measures are identical for both the sub-periods.

Overall, for wind data, there is differences between the results found between UCM simulations and the observed data. The simulations where the UCMs were used have poor skill when compared to the control simulations where the model skill for simulating both wind components can be considered high, according to the previously defined skill criteria.

7.3.2 Radiosonde Observations

Figure 7.12 shows the Taylor diagram and combined errors chart for a temperature profile taken from radiosonde data for the simulated period. One can see that the model has high skill in repro-

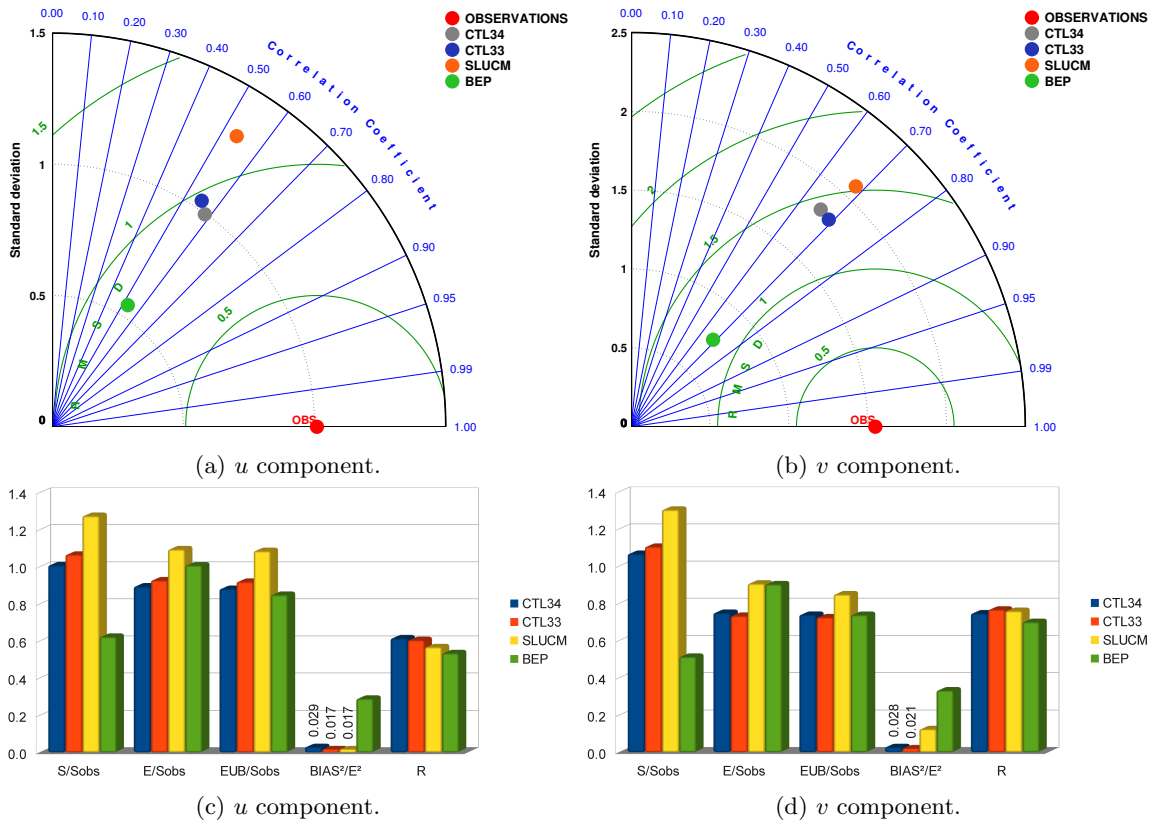


Figure 7.11: Taylor diagram for (a) *u* and, (b) *v* wind components and combined error chart for (c) *u* and (d) *v* wind components for all the simulated period.

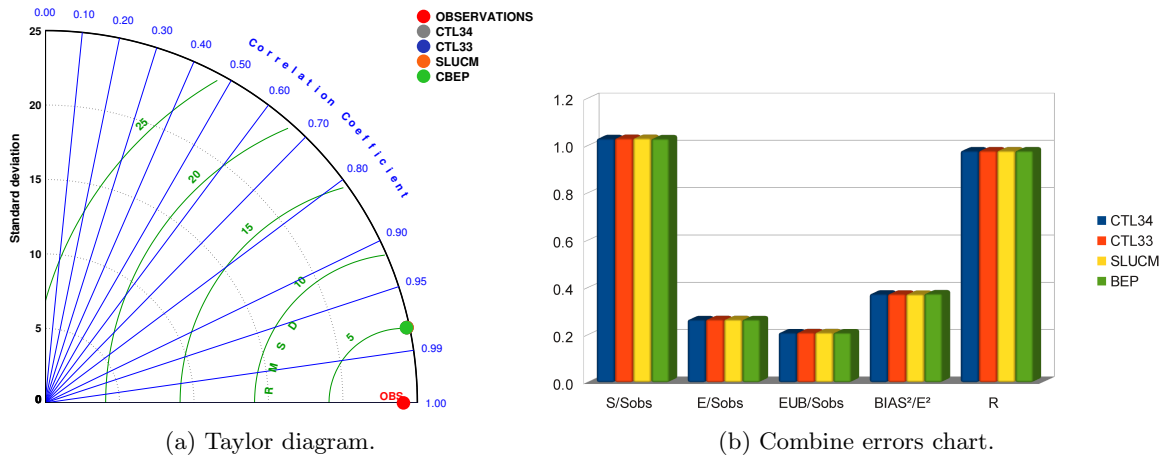


Figure 7.12: Taylor diagram and combined errors chart for temperature profile taken from radiosonde data for all the simulated period.

ducing the vertical temperature profile in every simulation and shows little differences between the simulations. In fact, the performance measures are quite identical between them.

As seen for temperature profile data, the performance measures for the wind flow profile results - not shown - are identical between simulations and little change in model skill between them can be observed. Still, despite the small amplitude errors and high correlation between the observed and modelled data (> 0.70), the observed variability is not well represented by the model. In addition, for this atmospheric property, the model performs better simulating the *u* wind component, which indicates that the model may miss represent the wind direction at higher levels of the troposphere.

In the previous Section, large differences for the PBL height between simulations have been identified.

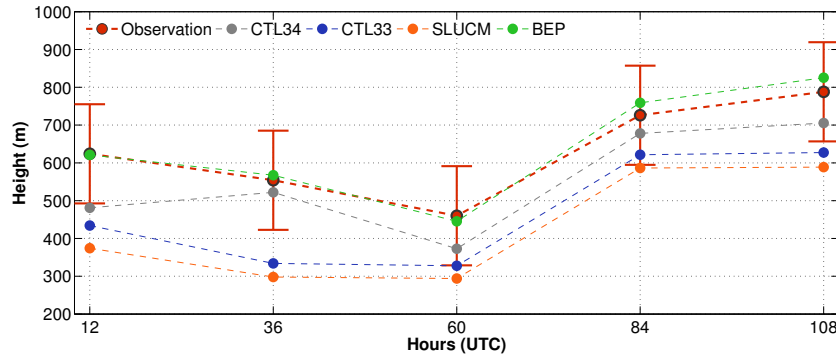


Figure 7.13: Time series of PBL height for observed data and its respective standard deviation (red) and for CTL34 (grey), CTL33 (blue), SLUCM (orange) and BEP (green) simulation.

Figure 7.13 shows the time series of PBL height for observed data and its respective standard deviation and for CTL34, CTL33, SLUCM and BEP. The observed PBL height variability is present in all simulations. However, only the BEP simulation represents closely the PBL height values found in the observed data while all other simulations present lower values of PBL height than the observed. This result may indicate that BEP simulation better describes the observed turbulent fluxes, despite its poor representation of surface temperature and wind. Therefore, considering the analysis performed in this section, one may conclude that there is no enhancement of model skill performance when using any of the tested UCMs for this case study.

7.4 Synthesis

The second Part of the present work focuses on the WRF sensitivity coupling with an Urban Canopy Model - UCM - when simulating atmospheric conditions over an urban area under anticyclonic conditions. The chosen event occurred between July 29th and August 3^{ed} 2010 over the Lisbon Region, the largest Portuguese city. The use of the CORINE land use data allowed the implementation of two UCMs - SLUCM and BEP - with distinctive characteristics from the parametrisation used in WRF model for the flow simulation in the lowest model level. Three different urban categories - high density residential, low density residential and commercial and transportation - were used, to which adequate parameters to fit the Lisbon City geometry were chosen.

When running the numerical simulations for the desired study period, with the configuration suggested by Ferreira (2007), some instabilities were created due to high values of vertical wind component at the top of the model. Hence, a different parametrisation set was applied, together with different filtering options. These instabilities may have been due to intense gravity wave activity generated in the domain.

This anticyclonic case study was divided into two sub-periods with distinct features - high temperatures with low wind flow and lower temperatures with strong wind flow. Comparing the results of the UCM simulations with their control simulations, changes in 2-m temperature were found. For both UCMs tested, a cooling effect was observed within the urban area. This cooling effect may originate from evapotranspiration processes, as the urban parameters chosen for the urban categories declared a higher amount of green areas than the one considered by the NOAA LSM in the control simulations. In addition, the wind flow analysis showed that drag and momentum exchange over the urban surface were different in both the UCMs. The SLUCM simulation was characterised by an intensification of wind flow when compared to the control simulation. On the contrary, the BEP simulation displayed a weakening of flow intensity. Moreover, it was possible to observe that there is a decrease of the TKE produced near the surface in the SLUCM simulation and a slight increase of TKE in the BEP simulation, which may indicate that the wind flow weakening in this simulation may result due to the interaction with turbulent processes of the urban region. Nonetheless, it was also verified that processes occurring in the UC can interact with the generation of gravity waves, changing their phase

and amplitude.

To evaluate which simulation represents well the observed data, the model results were compared against the observed data in two surface and one radiosonde stations. This comparison showed that all simulations have high skill when simulating 2-m temperature and a good model performance was also found for wind flow. However, no improvement was found in the model skill when using any of the studied UCMs. In fact, deterioration of model skill occurred when using SLUCM and BEP UCMs. When comparing the results to radiosonde observed data, it was seen that there is a high skill simulating temperature and wind profiles for every simulation. Furthermore, no differences in performance measures between the simulations were found.

To assess if the simulated turbulent processes are being well reproduced by the model, the comparison between the simulated and PBL height, derived from observations, was performed. The results showed that BEP simulation reproduce best the observed PBL height. All other simulations, showed values of PBL height that are lower than the observed. SLUCM simulation presented the greatest difference.

From the above results it can be inferred that, for this case study, and with the set of parametrizations chosen, the use of an UCM does not improve model performance to simulate 2-m temperature and mean surface wind flow. However, BEP UCM shows better results reproducing the observed PBL height, which may be associated to better representation of turbulent processes that occur within the UC. To better understand the advantages of the UCMs a broader study, using multi-event analysis and a better representation of urban geometry should be performed, due to the high sensitivity of the urban parameters defined in each UCM, as shown by Wang et al. (2011).

Chapter 8

Concluding Remarks

The availability of high resolution datasets for topography - SRTM and ASTER - and land use - CORINE land cover - made possible the improvement of lower boundary conditions specification in atmospheric models, as well as the use of new features such as UCMs. The present work evaluates the usage of these datasets in the WRF model. In order to achieve this, two case studies in which these datasets play a crucial role were considered.

The first part of this study consider the extreme precipitation event of orographic nature that occurred over Madeira Island in February 20th, 2010. This simulation has been compared with a control simulation where the WRF default topography (GTOPO30) and land use (USGS 30) datasets have been used. The use of high resolution topography datasets showed a reduction of near surface wind speed in Madeira Island ridge and an intensification in valleys. Also, the leeward region presented differences which may be associated with wind flow paths. For precipitation it was found that there is an increase of precipitation amounts in the mountainous region and a decrease of precipitation amounts in the valleys for SRTM and ASTER simulations. On the other hand, for CORINE simulation little differences were found.

When evaluating the simulated results against the observations it was found that, for this case study and for the new datasets there is little enhancement of overall model skill in the simulation of near surface wind and precipitation. However, considering local skill scores, SRTM simulation presented improvement in model skill when simulating wind flow leeward and precipitation in windward region of Madeira Island.

The second Part of this work was focused on the study of model sensitivity to the coupling of two UCMs with the WRF model, namely the SLUCM and BEP. A period in which atmospheric conditions favoured the development of UHI effect over Lisbon Region was considered. The period chosen was between July 29th and August 3^{ed}, 2010. During this period the region was under the influence of an high pressure system, favouring strong surface heating and weak horizontal pressure gradients. For these simulations results showed that when using an UCM, differences in UCM parameters such as green fraction in urban categories can lead to a cooling of the urban area. Furthermore, it has been observed that the use of SLUCM results in an intensification of near surface wind speed whereas with BEP a decrease of near surface wind speed is observed, when both simulations are compared with their respective control simulation. These opposite results between UCMs show the importance of solving the complex processes that occur within the UC as BEP solves more complex physics processes than SLUCM. It was also shown that there is more TKE being produced over the urban area when using the BEP model and less TKE when the SLUCM is used. In addition, and given the atmospheric conditions of high static stability that were present in the simulated period, the development of gravity waves over the urban area was verified. Also, for these conditions, the interaction between the UCMs and gravity waves already present in the control simulations, lead to changes in the amplitude and phase of these waves.

These simulations have been compared with observed data. Little change to model skill was detected when using any of the UCMs. In fact, both simulations using an UCM showed a decrease of performance, according to the performance measures used here. However, only BEP was capable of better reproducing the observed PBL height for the simulated period.

The results obtained in this study are only valid for the two regions and case-studies considered. Similar simulations to evaluate the impact of the usage of high resolution lower boundary conditions, such as topography and land use, and UCMs, should be performed for other synoptic atmospheric conditions and regions. Also, other simulations should be performed to evaluate what is the set of physics parametrizations not considered here, such as radiation, convection, microphysics, land surface and boundary layer that give the best overall model skill.

Bibliography

- Alcoforado, M. and Andrade, H. (2006). Nocturnal urban heat island in lisbon (portugal): main features and modelling attempts. *Theoretical and applied climatology*, 84(1):151–159.
- Alcoforado, M., Andrade, H., Lopes, A., and Vasconcelos, J. (2009). Application of climatic guidelines to urban planning: the example of lisbon (portugal). *Landscape and Urban Planning*, 90(1):56–65.
- Bischoff-Gauß, I., Kalthoff, N., and Fiebig-Wittmaack, M. (2006). The influence of a storage lake in the arid elqui valley in chile on local climate. *Theoretical and applied climatology*, 85(3):227–241.
- Bond, N. and Stabeno, P. (1998). Analysis of surface winds in shelikof strait, alaska, using moored buoy observations*. *Weather and forecasting*, 13(3):547–559.
- Bossard, M., Feranec, J., and Otahel, J. (2000). Corine land cover technical guide addendum 2000. Technical report, European Environment Agency.
- Bougeault, P. and Lacarrere, P. (1989). Parameterization of orography-induced turbulence in a mesobeta-scale model. *Monthly Weather Review*, 117(8):1872–1890.
- Chen, F. and Dudhia, J. (2001). Coupling an advanced landsurface/hydrology model with the penn state/ncar mm5 modeling system. part i: Model description and implementation. *Monthly Weather Review*, 129:569–585.
- Chen, F., Warner, T., and Manning, K. (2001). Sensitivity of orographic moist convection to landscape variability: A study of the buffalo creek, colorado, flash flood case of 1996. *Journal of the atmospheric sciences*, 58(21):3204–3223.
- Chin, H., Leach, M., Sugiyama, G., Leone Jr, J., Walker, H., Nasstrom, J., and Brown, M. (2005). Evaluation of an urban canopy parameterization in a mesoscale model using vtmx and urban 2000 data. *Monthly weather review*, 133(7):2043–2068.
- Ching, J., Brown, M., McPherson, T., Burian, S., Chen, F., Cionco, R., Hanna, A., Hultgren, T., Sailor, D., Taha, H., et al. (2009). National urban database and access portal tool. *Bulletin of the American Meteorological Society*, 90(8):1157–1168.
- Colle, B. (2004). Sensitivity of orographic precipitation to changing ambient conditions and terrain geometries: An idealized modeling perspective. *Journal of the atmospheric sciences*, 61(5):588–606.
- Colle, B. and Mass, C. (1998). Windstorms along the western side of the washington cascade mountains. part i: A high-resolution observational and modeling study of the 12 february 1995 event. *Monthly weather review*, 126(1):28–52.
- Couto, F., Salgado, R., and Costa, M. (2012). Analysis of intense rainfall events on madeira island during the 2009/2010 winter. *Nat. Hazards Earth Syst. Sci*, 12:2225–2240.
- Dudhia, J. (1989). Numerical study of convection observed during the winter monsoon experiment using a mesoscale two-dimensional model. *Journal of the Atmospheric Sciences*, 46(20):3077–3107.
- Elementi, M., Marsigli, C., and Paccagnella, T. (2005). High resolution forecast of heavy precipitation with lokal modell: analysis of two case studies in the alpine area. *Natural Hazards and Earth System Science*, 5(4):593–602.
- Farr, T. G., Rosen, P. A., Caro, E., Crippen, R., Duren, R., Hensley, S., Kobrick, M., Paller, M., Rodriguez, E., Roth, L., Seal, D., Shaffer, S., Shimada, J., Umland, J., Werner, M., Oskin, M., Burbank, D., and Alsdorf, D. (2007). The shuttle radar topography mission. *Reviews of Geophysics*, 45:1–33.

- Ferreira, A. P. (2007). Sensibilidade as parametrizacoes fisicas do wrf nas previsoos a superficie em portugal continental. relatorio de estagio em meteorologia e oceanografia fisica.
- Gemmill, W., Katz, B., and Li, X. (2007). Daily real-time, global sea surface temperature–high resolution analysis: Rtg_sst_hr. ncep/emc office note.
- Ghafarian, P., Azadi, M., Meshkatee, A. H., and Farahani, M. M. (2012). Numerical simulation of the impact of anatolian and caucasus mountains on the precipitation distribution over the black sea. *Natural Hazards and Earth System Science*, 12(3):607–613.
- Grawe, D., Thompson, H., Salmond, J., Cai, X., and Schlünzen, K. (2012). Modelling the impact of urbanisation on regional climate in the greater london area. *International Journal of Climatology*.
- Grumm, R. (2010). The madeira island floods of 20 february 2010.
- Holton, J. (2004). *An introduction to dynamic meteorology*, volume 1. Academic press.
- Hong, S. Y. and Lim, J. O. J. (2006). The wrf single-moment 6-class microphysics scheme (wsm6). *Journal of the Korean Meteorological Society*, 42:129–151.
- Janjić, Z. (2002). Nonsingular implementation of the mellor–yamada level 2.5 scheme in the ncep meso model. *NCEP Office Note*, 437:61.
- Janjic, Z. I. (1990). The step-mountain coordinate: physical package. *Monthly Weather Review*, 118:1429–1443.
- Jiang, Q. (2003). Moist dynamics and orographic precipitation. *Tellus A*, 55(4):301–316.
- Kain, J. (1993). Convective parameterization for mesoscale models: The kain–fritsch scheme. *The representation of cumulus convection in numerical models, Meteor. Monogr*, 46:165–170.
- Koletsis, I., Lagouvardos, K., Kotroni, V., and Bartzokas, A. (2010). The interaction of northern wind flow with the complex topography of crete island part 2: Numerical study. *Natural Hazards and Earth System Sciences*, 10:1115–1127.
- Kunz, M. and Kottmeier, C. (2006a). Orographic enhancement of precipitation over low mountain ranges. part i: Model formulation and idealized simulations. *Journal of applied meteorology and climatology*, 45(8):1025–1040.
- Kunz, M. and Kottmeier, C. (2006b). Orographic enhancement of precipitation over low mountain ranges. part ii: Simulations of heavy precipitation events over southwest germany. *Journal of applied meteorology and climatology*, 45(8):1041–1055.
- Kusaka, H. and Kimura, F. (2004). Coupling a single-layer urban canopy model with a simple atmospheric model: Impact on urban heat island simulation for an idealized case. *Journal of the Meteorological Society of Japan*, 82(1):67–80.
- Kusaka, H., Kondo, H., Kikegawa, Y., and Kimura, F. (2001). A simple single-layer urban canopy model for atmospheric models: Comparison with multi-layer and slab models. *Boundary-Layer Meteorology*, 101(3):329–358.
- Landsberg, H. (1981). *The urban climate*, volume 28. Academic press.
- Lee, S., Kim, S., Angevine, W., Bianco, L., McKeen, S., Senff, C., Trainer, M., Tucker, S., and Zamora, R. (2010). Evaluation of urban surface parameterizations in the wrf model using measurements during the texas air quality study 2006 field campaign. *Atmospheric Chemistry & Physics Discussions*, 10:25033–25080.
- Lemonsu, A., Belair, S., and Mailhot, J. (2009). The new canadian urban modelling system: Evaluation for two cases from the joint urban 2003 oklahoma city experiment. *Boundary-layer meteorology*, 133(1):47–70.

- Lin, Y., Farley, R., and Orville, H. (1983). Bulk parameterization of the snow field in a cloud model. *Journal of Climate and Applied Meteorology*, 22(6):1065–1092.
- Lo, J., Lau, A., Chen, F., Fung, J., and Leung, K. (2007). Urban modification in a mesoscale model and the effects on the local circulation in the pearl river delta region. *Journal of applied meteorology and climatology*, 46(4):457–476.
- Luna, T., Rocha, A., Carvalho, A., Ferreira, J., and Sousa, J. (2011). Modelling the extreme precipitation event over madeira island on 20 february 2010. *Nat. Hazards Earth Syst. Sci*, 11:2437–2452.
- Martilli, A., Clappier, A., and Rotach, M. (2002). An urban surface exchange parameterisation for mesoscale models. *Boundary-Layer Meteorology*, 104(2):261–304.
- Maussion, F., Scherer, D., Finkelnburg, R., Richters, J., Yang, W., and Yao, T. (2010). Wrf simulation of a precipitation event over the tibetan plateau, china—an assessment using remote sensing and ground observations. *Hydrology and Earth System Sciences Discussions*, 7:3551–3589.
- M.D., C. and Suarez, M. (2001). A thermal infrared radiation parameterization for atmospheric studies. *NASA/TM*, 2001-104606(19):55.
- Meng, W., Zhang, Y., Li, J., Lin, W., Dai, G., and Li, H. (2010). Application of wrf/ucm in the simulation of a heat wave event and urban heat island around guangzhou city. *Journal of Tropical Meteorology*, 3:003.
- Mlawer, E. J., Taubman, S. J., Brown, P. D. and Lacono, M. J., and Clough, S. A. (1997). Radiative transfer for inhomogeneous atmosphere: Rrtm, a validated correlated-k model for the long-wave. *Journal of Geophysical Research*, 102 (D14):16663–16682.
- Nadeau, D., Brutsaert, W., Parlange, M., Bou-Zeid, E., Barrenetxea, G., Couach, O., Boldi, M., Selker, J., and Vetterli, M. (2009). Estimation of urban sensible heat flux using a dense wireless network of observations. *Environmental fluid mechanics*, 9(6):635–653.
- NCEP (2003). The gfs atmospheric model. ncep office note 442, global climate and weather modeling branch. Technical report, EMC, Cam Springs Maryland.
- Ohashi, Y. and Kida, H. (2002). Local circulations developed in the vicinity of both coastal and inland urban areas: A numerical study with a mesoscale atmospheric model. *Journal of Applied Meteorology*, 41(1):30–45.
- Pielke, R. (2002). *Mesoscale meteorological modeling*, volume 78. Academic Pr.
- Pineda, N., Jorba, O., Jorge, J., and Baldasano, J. (2004). Using noaa avhrr and spot vgt data to estimate surface parameters: application to a mesoscale meteorological model. *International Journal of Remote Sensing*, 25(1):129–143.
- Rao, M., Castracane, P., Casadio, S., Fuá, D., and Fiocco, G. (2004). Observations of atmospheric solitary waves in the urban boundary layer. *Boundary-layer meteorology*, 111(1):85–108.
- Ren, C., Ng, E., and Katzschner, L. (2011). Urban climatic map studies: a review. *International Journal of Climatology*, 31(15):2213–2233.
- Salamanca, F., Martilli, A., Tewari, M., and Chen, F. (2011). A study of the urban boundary layer using different urban parameterizations and high-resolution urban canopy parameters with wrf. *Journal of Applied Meteorology and Climatology*, 50(5):1107–1128.
- Shi, X., Wang, Y., and Xu, X. (2008). Effect of mesoscale topography over the tibetan plateau on summer precipitation in china: A regional model study. *Geophys. Res. Lett*, 35:L19707.
- Skamarock, W. C., Klemp, J. B., Dudhia, J., Gill, D. O., Barke, D. M., Wang, W., and Powers, J. G. (2008). A description of the advance reaserch wrf version 3. Technical report, NCAR.
- Stull, R. (1988). *An introduction to boundary layer meteorology*, volume 13. Springer.

- Tachikawa, T., Hato, M., Kaku, M., and Iwasaki, A. (2011). Characteristics of aster gdem version 2. In *Geoscience and Remote Sensing Symposium (IGARSS), 2011 IEEE International*, pages 3657–3660. IEEE.
- Thompson, G., Rasmussen, R., and Manning, K. (2004). Explicit forecasts of winter precipitation using an improved bulk microphysics scheme. part i: Description and sensitivity analysis. *Monthly Weather Review*, 132(2):519–542.
- Tomassetti, B., Giorgi, F., Verdecchia, M., and Visconti, G. (2003). Regional model simulation of the hydrometeorological effects of the fucino lake on the surrounding region. *Annales Geophysicae*, 21:2219–2232.
- Viterbo, P. and Betts, A. K. (1999). Impact of the ecmwf reanalysis soil water on forecasts of the july 1993 mississippi flood. *Journal of Geophysical Research*, 104:1936119366.
- Vrochidou, A. and Tsanis, I. (2012). Assessing precipitation distribution impacts on droughts on the island of crete. *Nat. Hazards Earth Syst. Sci*, 12:1159–1171.
- Wang, Z., Bou-Zeid, E., Au, S., and Smith, J. (2011). Analyzing the sensitivity of wrf’s single-layer urban canopy model to parameter uncertainty using advanced monte carlo simulation. *Journal of Applied Meteorology and Climatology*, 50(9):1795–1814.
- Weigel, A. P., Chow, F. K., and Rotach, M. W. (2007). The effect of mountainous topography on moisture exchange between the surface and the free atmosphere. *Boundary-Layer Meteorology*, 125:227 – 244.
- Wyszogrodzki, A., Miao, S., and Chen, F. (2012). Evaluation of the coupling between mesoscale-wrf and les–eulag models for simulating fine-scale urban dispersion. *Atmospheric Research*.
- Xue, Y., Fennessy, M., and Sellers, P. (1996). Impact of vegetation properties on us summer weather prediction. *Journal of Geophysical Research. D. Atmospheres*, 101:7419–7430.